PHYSICAL REVIEW D **90,** 075001 (2014)

Fingerprinting nonminimal Higgs sectors

Shinya Kanemura,[1,*] Koji Tsumura,[2,†] Kei Yagyu,[3,‡] and Hiroshi Yokoya[1,§]
[1]*Department of Physics, University of Toyama, Toyama 930-8555, Japan*
[2]*Division of Physics and Astronomy, Kyoto University, Kyoto 606-8502, Japan*
[3]*Department of Physics, National Central University, Chungli 32001, Taiwan*
(Received 12 June 2014; published 1 October 2014)

After the discovery of the standard model-like Higgs boson at the LHC, the structure of the Higgs sector remains unknown. We discuss how it can be determined by the combination of direct and indirect searches for additional Higgs bosons at future collider experiments. First of all, we evaluate expected excluded regions for the mass of additional neutral Higgs bosons from direct searches at the LHC with the 14 TeV collision energy in the two Higgs doublet models with a softly broken Z_2 symmetry. Second, precision measurements of the Higgs boson couplings at future experiments can be used for the indirect search of extended Higgs sectors if the measured coupling constant with the gauge boson slightly deviates from the standard model value. In particular, in the two Higgs doublet model with the softly broken discrete symmetry, there are four types of Yukawa interactions, so that they can be discriminated by measuring the pattern of deviations in Yukawa coupling constants. Furthermore, we can fingerprint various extended Higgs sectors with future precision data by detecting the pattern of deviations in the coupling constants of the standard model-like Higgs boson. We demonstrate how the pattern of deviations can be different among various Higgs sectors that predict the electroweak rho parameter to be unity, such as models with additional an isospin singlet, a doublet, triplets, or a septet. We conclude that, as long as the gauge coupling constant of the Higgs boson slightly differs from the standard model prediction but is enough to be detected at the LHC and its high-luminosity run or at the International Linear Collider, we can identify the nonminimal Higgs sector even without direct discovery of additional Higgs bosons at the LHC.

DOI: 10.1103/PhysRevD.90.075001 PACS numbers: 12.60.Fr

I. INTRODUCTION

The new particle discovered at the LHC in 2012 was identified as a Higgs boson [1]. With the current LHC data, its measured properties are consistent with those of the Higgs boson in the standard model (SM) [2–4]. On the other hand, so far, no evidence for new physics beyond the SM has been found directly at the LHC. Therefore, our standard picture for high-energy particle phenomena, which is based on the gauge theory with spontaneous symmetry breaking, seems successful.

However, it has been well known that the Higgs sector in the SM is problematic from the theoretical viewpoint. First of all, the existence of the scalar boson causes the hierarchy problem [5–7] so that many physicists try to understand the essence of the Higgs boson, e.g., elementary or composite particle. To solve the hierarchy problem, several scenarios for the new paradigm have been introduced such as supersymmetry, dynamical symmetry breaking, and extra dimensions. Each of them gives a different answer for the question of the essence of the Higgs boson. Second, there is no principle for the structure of the Higgs sector so that the minimal Higgs sector adopted in the SM is just an assumption. There are many possibilities of nonminimal Higgs sectors with additional scalar fields such as singlets, doublets, and triplets. A model based on the above-discussed paradigms can predict the specific structure and property of the Higgs sector. For example, the minimal supersymmetric SM (MSSM) predicts the Higgs sector with two isospin doublet scalar fields [8,9]. In addition, nonminimal Higgs sectors can also be introduced in new physics models to explain the origin of neutrino masses, the existence of dark matter and baryon asymmetry of the Universe, etc., which cannot be explained in the SM. Each new physics model predicts a characteristic structure for the Higgs sector. Therefore, if the Higgs sector is determined by experiments in the future, the new physics scenario can be selected from many candidates.

To probe the extended Higgs sectors, the simplest way is to directly search for additional Higgs bosons such as the second scalar boson. By measuring its properties, e.g., the mass, the electric charge, the spin, and the parity, important information to reconstruct the Higgs sector can be extracted. Nonobservation of the second Higgs boson gives the experimental constraint on the parameter space

*kanemu@sci.u-toyama.ac.jp
†ko2@gauge.scphys.kyoto-u.ac.jp
‡keiyagyu@ncu.edu.tw
§hyokoya@sci.u-toyama.ac.jp

in the Higgs sector. Current bounds from searches for additional Higgs bosons at the LHC with the collision energy of 7 and 8 TeV can be found in Refs. [4,10–19].

In addition to the direct search results, precision measurements of various low-energy observables can be an indirect search for extended Higgs sectors, since the existence of additional Higgs multiplets can affect them. The electroweak rho parameter defined in terms of the masses of the W boson m_W and the Z boson m_Z, and the weak mixing angle θ_W by

$$\rho = \frac{m_W^2}{m_Z^2 \cos^2\theta_W}, \tag{1}$$

is one of the most important tools to constrain the structure of the Higgs sector, for which the experimental value is very close to unity; i.e., $\rho_{\rm exp} = 1.0004^{+0.0003}_{-0.0004}$ [20]. In the SM, the rho parameter is predicted to be unity at the tree level. In general, in extended Higgs sectors, predicted values for the rho parameter can deviate from unity. In the Higgs sector with an arbitrary number of scalar fields ϕ_i (a hypercharge Y_i and an isospin T_i) with vacuum expectation values (VEVs) v_i, the rho parameter is calculated at the tree level by [9]

$$\rho_{\rm tree} = \frac{\sum_i [T_i(T_i+1) - Y_i^2] v_i^2}{2\sum_i Y_i^2 v_i^2}. \tag{2}$$

From Eq. (2), an additional VEV of a Higgs field satisfying $T_i(T_i+1) - 3Y_i^2 = 0$ does not change the value of the rho parameter from the SM.[1] A VEV of a Higgs multiplet without satisfying the above equation, e.g., a triplet Higgs field, deviates $\rho_{\rm tree}$ from unity so that we need fine-tuning for such a VEV to avoid the constraint from $\rho_{\rm exp}$. However, even if the above equation is not satisfied, by allowing an alignment among VEVs, we can keep $\rho_{\rm tree} = 1$. The simplest realization is known as the Georgi-Machacek (GM) model [22] for which the Higgs sector is composed of additional real and complex triplet fields with $Y_i = 0$ and $Y_i = 1$, respectively.

The above discussion is very useful to discriminate extended Higgs sectors. However, the rho parameter has been measured quite precisely so that we need to take into account quantum effects to the rho parameter. Let us discuss how the rho parameter is modified at the one-loop level. The deviation of the rho parameter from unity measures the violation of the custodial $SU(2)_V$ symmetry [5,7,23] in the sector of particles in the loop.[2] For example, in the Yukawa Lagrangian, the custodial symmetry is broken by the mass splitting between the top and bottom quarks. As a result, the deviation of the rho parameter from unity $\Delta\rho \equiv \rho - 1$ due to the loop contribution of the top and bottom quarks takes a form of $\Delta\rho \propto (m_t - m_b)^2$. In fact, since $m_t \gg m_b$, there remains m_t^2 dependence in $\Delta\rho$. On the other hand, the Higgs potential in the SM respects the custodial symmetry so that the Higgs boson loop contribution is at most the logarithmic dependence of the Higgs boson mass through the hypercharge gauge interaction. However, in general, the custodial symmetry is broken in extended Higgs sectors. For example, in two Higgs doublet models (THDMs), the mass splitting between singly charged Higgs bosons and a CP-odd Higgs boson gives a quadratic mass dependence similarly to the top and bottom quark contributions in $\Delta\rho$ [29–33]. Therefore, a sizable amount of the mass difference has already been excluded [34,35]. In the above way, we can take bounds on various physical parameters by comparing precisely measured observables with theory predictions with radiative corrections.

Experimental data for flavor changing neutral current (FCNC) processes such as $K_L^0 \to \mu^+\mu^-$ and the B^0-$\bar{B}^0$ mixing strongly constrain extended Higgs sectors with multidoublet structures. The way to avoid such dangerous FCNC processes at the tree level is to assign a different quantum number for each Higgs doublet. Consequently, each quark or lepton can obtain its mass from only one Higgs doublet just like in the SM, and therefore the model escapes FCNC processes at the tree level. In the THDM, for example, this can be achieved by imposing a discrete Z_2 symmetry, which can be softly broken in the potential, to the model [36] as the simplest way. There are four independent types of Yukawa interactions under the Z_2 symmetry [37–39], which are called type-I, type-II, type-X, and type-Y [40].[3,4]

[1] Although there is an infinite number of solutions for the above equation, larger isospin representation fields cause violation of perturbative unitarity [21]. Therefore, only the three possibilities can be substantially considered, i.e., isospin singlets with $Y_i = 0$, doublets with $Y_i = 1/2$, and septets with $Y_i = 2$. The next possibility to the septet representation is isospin 26-plet with $Y_i = 15/2$.

[2] In models with $\rho_{\rm tree} \neq 1$, we need a different prescription for the calculation of the radiative corrections to the rho parameter from that in models with $\rho_{\rm tree} = 1$, because of an additional input parameter in the electroweak sector. In the Higgs sector with a real triplet Higgs field with $Y = 0$, one-loop corrections to the rho parameter have been calculated in Refs. [24,25]. That has been applied to the Higgs sector with a complex triplet Higgs field with $Y = 1$ in Refs. [26,27]. In the GM model, although $\rho_{\rm tree} = 1$ can be satisfied, a similar prescription in models with $\rho_{\rm tree} \neq 1$ is necessary due to the VEV alignment [28].

[3] The type-X (type-Y) THDM is referred to as the type-IV (type-III) THDM in Ref. [37], type-I' (type-II') THDM in Refs. [38,39], and the lepton-specific (flipped) THDM in Refs. [41–43]. Because the term "type-III" is sometimes used for the THDM with tree-level FCNCs [44], we adopt the terms "type-X" and "type-Y" to avoid confusion.

[4] If we introduce right-handed neutrinos, four more types of Yukawa interactions can be defined. In particular, if one of the two doublets gives Dirac neutrino masses, and another one gives masses of all the other fermions, it is known as the neutrinophilic THDM [45].

How can we explore extended Higgs sectors? It is important to understand that, in general, a new scale M is introduced in extended Higgs sectors, which is irrelevant to the VEV of the Higgs boson. When M is much larger than the TeV scale, the mass of the second Higgs boson is approximately given by M. In this case, the second Higgs boson is too heavy to be discovered directly at the LHC. In addition, the indirect effect of new particles decouples from the low-energy observables [46] such as the coupling constants of the discovered Higgs boson. However, if M is as high as the TeV scale, there can be two possibilities in searches for additional Higgs bosons. The first possibility is that the second Higgs boson can be discovered directly at the LHC. In this case, the properties can be directly measured at the LHC, and the useful information to determine the structure of the Higgs sector can also be obtained at the High Luminosity (HL)-LHC [47–49]. The second possibility is that it cannot be discovered directly, but its indirect effect on the Higgs couplings can be significant and thus detectable by precision measurements at the HL-LHC and at the International Linear Collider (ILC) [50]. It goes without saying that, in order to realize the second possibility, a small but detectable mixing between the SM-like Higgs boson and an additional Higgs boson is required. In this case, in addition to obtaining information on the mass of the second Higgs boson, the structure of the Higgs sector could be determined without the direct discovery by finding the pattern in deviations in various Higgs boson couplings [51,52]. On the other hand, if M stays at the electroweak scale, a large mixing between the SM-like Higgs boson and an additional Higgs boson can occur, and the Higgs boson couplings can deviate significantly from the SM values. If the last scenario is realized, both the direct search and the indirect search are possible to determine the Higgs sector. The direct search for additional Higgs bosons in THDMs at the LHC was discussed in Refs. [53–58] after the discovery of the Higgs boson. The complementarity of additional Higgs boson searches at the LHC and at the ILC was recently discussed in Ref. [59].

In this paper, we discuss how the structure of the Higgs sector can be determined at the LHC and at the ILC. In particular, we shed light on complementarity of direct searches of additional Higgs bosons at the upcoming 13 TeV or 14 TeV run of the LHC and precision measurements of the coupling constants of the discovered Higgs boson at future collider experiments. We consider extended Higgs sectors that satisfy $\rho_{\text{tree}} = 1$ without predicting FCNCs at the tree level, i.e., the THDM with the softly broken Z_2 symmetry, the doublet-singlet model [60], the GM model [22], and the doublet-septet model [61–63]. For the THDM, we discuss the four types of Yukawa interaction. We at first give a detailed explanation for properties in the THDMs such as the decay branching ratio, perturbative unitarity, and vacuum stability. We then analyze the direct search for additional neutral Higgs bosons at the LHC. The expected excluded regions on the mass of extra neutral Higgs bosons are shown assuming the 14 TeV energy at the LHC.[5] Next, as the indirect search, we show various patterns of deviations in the gauge interaction hVV and the Yukawa interactions $hf\bar{f}$ of the SM-like Higgs boson h from the SM predictions. We show the deviation in the $hf\bar{f}$ couplings in the THDMs. For the rest models, we also show those in the $hf\bar{f}$ and hVV couplings, where these models predict universal modifications for the $hf\bar{f}$ couplings. We use the latest results of allowed values of the Higgs boson couplings that have been obtained from the global fit to all Higgs data [64] in order to compare the various prediction of deviations in the Higgs boson couplings.[6]

This paper is organized as follows. In Sec. II, we define the Higgs potential and Yukawa Lagrangian in the THDM with the softly broken Z_2 symmetry. After we derive the Yukawa couplings in the four types, we discuss the decay branching ratios of the Higgs bosons. The bounds from unitarity and vacuum stability are also discussed. In Sec. III, we study the direct search for the additional Higgs bosons at the LHC. In Sec. IV, we present expected accuracy of the precise measurement of the Higgs boson couplings at the ILC, and then we discuss how the deviation in the SM-like Higgs boson couplings are calculated in the THDMs and models with universal Yukawa couplings. Complementarity between the direct search and the indirect search at the LHC and at the ILC is discussed in Sec. IV. The conclusion is summarized in Sec. V.

II. TWO HIGGS DOUBLET MODEL

A. Lagrangian

The Higgs potential of the THDM under the softly broken Z_2 symmetry to avoid FCNC at the tree level and the CP invariance is given by [9,43,65,66]

$$\begin{aligned} V_{\text{THDM}} = {} & m_1^2|\Phi_1|^2 + m_2^2|\Phi_2|^2 - m_3^2(\Phi_1^\dagger\Phi_2 + \text{H.c.}) \\ & + \frac{1}{2}\lambda_1|\Phi_1|^4 + \frac{1}{2}\lambda_2|\Phi_2|^4 + \lambda_3|\Phi_1|^2|\Phi_2|^2 \\ & + \lambda_4|\Phi_1^\dagger\Phi_2|^2 + \frac{1}{2}\lambda_5[(\Phi_1^\dagger\Phi_2)^2 + \text{H.c.}], \end{aligned} \tag{3}$$

where Φ_1 and Φ_2 are the isospin doublet scalar fields with $Y = 1/2$ for which Z_2 transformation is given as $\Phi_1 \to +\Phi_1$ and $\Phi_2 \to -\Phi_2$. The two Higgs doublet fields can be parametrized as

[5] In Fig. 1.20 in the ILC Higgs White Paper [51], we have shown the expected excluded parameter space in the type-II and type-X THDMs at the LHC. We update this analysis with more detailed explanations.

[6] In Figs. 1.17 and 1.18 in the ILC Higgs White Paper [51], we have shown the deviation in the $hf\bar{f}$ and hVV couplings in the THDMs and in the models with universal modification of the $hf\bar{f}$ couplings. We update the plots for the $hf\bar{f}$ and hVV couplings with more detailed explanations by using the latest data [64].

TABLE I. Four types of the charge assignment of the Z_2 symmetry.

	Φ_1	Φ_2	u_R	d_R	ℓ_R	Q_L, L_L
Type-I	+	−	−	−	−	+
Type-II	+	−	−	+	+	+
Type-X	+	−	−	−	+	+
Type-Y	+	−	−	+	−	+

$$\Phi_i = \begin{bmatrix} w_i^+ \\ \frac{1}{\sqrt{2}}(h_i + v_i + iz_i) \end{bmatrix}, \quad (i = 1, 2), \tag{4}$$

where v_1 and v_2 are the VEVs of two doublet fields. They are related to the Fermi constant G_F by $v^2 \equiv v_1^2 + v_2^2 = (\sqrt{2}G_F)^{-1}$. The ratio of the two VEVs is defined as $\tan\beta = v_2/v_1$.

The mass eigenstates for the scalar bosons are obtained by the orthogonal transformations as

$$\begin{pmatrix} w_1^\pm \\ w_2^\pm \end{pmatrix} = R(\beta)\begin{pmatrix} G^\pm \\ H^\pm \end{pmatrix}, \qquad \begin{pmatrix} z_1 \\ z_2 \end{pmatrix} = R(\beta)\begin{pmatrix} G^0 \\ A \end{pmatrix},$$
$$\begin{pmatrix} h_1 \\ h_2 \end{pmatrix} = R(\alpha)\begin{pmatrix} H \\ h \end{pmatrix},$$
$$\text{with} \quad R(\theta) = \begin{pmatrix} \cos\theta & -\sin\theta \\ \sin\theta & \cos\theta \end{pmatrix}, \tag{5}$$

where $G^\pm$ and G^0 are the Nambu-Goldstone bosons absorbed by the longitudinal component of $W^\pm$ and Z, respectively. The masses of $H^\pm$ and A are calculated as

$$m_{H^+}^2 = M^2 - \frac{v^2}{2}(\lambda_4 + \lambda_5), \qquad m_A^2 = M^2 - v^2\lambda_5, \tag{6}$$

where $M^2 \equiv m_3^2/(\sin\beta\cos\beta)$ describes the soft breaking scale of the Z_2 symmetry [66]. The masses for the CP-even Higgs bosons h and H and the mixing angle α are given by

$$m_H^2 = \cos^2(\beta-\alpha)M_{11}^2 + \sin^2(\beta-\alpha)M_{22}^2 - \sin 2(\beta-\alpha)M_{12}^2, \tag{7}$$

$$m_h^2 = \sin^2(\beta-\alpha)M_{11}^2 + \cos^2(\beta-\alpha)M_{22}^2 + \sin 2(\beta-\alpha)M_{12}^2, \tag{8}$$

$$\tan 2(\beta-\alpha) = \frac{2M_{12}^2}{M_{22}^2 - M_{11}^2}, \tag{9}$$

where

$$M_{11}^2 = v^2(\lambda_1\cos^4\beta + \lambda_2\sin^4\beta) + \frac{v^2}{2}\bar{\lambda}\sin^2 2\beta, \tag{10}$$

$$M_{22}^2 = M^2 + v^2(\lambda_1 + \lambda_2 - 2\bar{\lambda})\sin^2\beta\cos^2\beta, \tag{11}$$

$$M_{12}^2 = \frac{v^2}{2}(-\lambda_1\cos^2\beta + \lambda_2\sin^2\beta)\sin 2\beta + \frac{v^2}{2}\bar{\lambda}\sin 2\beta\cos 2\beta, \tag{12}$$

with $\bar{\lambda} \equiv \lambda_3 + \lambda_4 + \lambda_5$. We define the range of $\beta - \alpha$ to be $[0, \pi/2]$ or $[\pi/2, \pi]$, which for a given positive value of $\sin(\beta-\alpha)$, $\cos(\beta-\alpha)$ is positive or negative, respectively.

The Yukawa Lagrangian under the Z_2 symmetry is given by

$$\mathcal{L}_{\rm THDM}^Y = -Y_u\overline{Q_L}\tilde{\Phi}_u u_R - Y_d\overline{Q_L}\Phi_d d_R - Y_\ell\overline{L_L}\Phi_\ell\ell_R + \text{H.c.}, \tag{13}$$

where $\Phi_{u,d,\ell}$ are either Φ_1 or Φ_2 and $\tilde{\Phi}_u = i\tau_2\Phi_u^*$. There are four independent ways of the charge assignment of the Z_2 symmetry as summarized in Table I, which are named type-I, type-II, type-X, and type-Y Yukawa interactions according to Ref. [40]. After we specify the types of Yukawa interactions, the Yukawa coupling constants are expressed in the mass eigenstate of the Higgs bosons as

$$\begin{aligned}\mathcal{L}_{\rm THDM}^Y = &-\sum_{f=u,d,e}\frac{m_F}{v}(\xi_h^f\bar{f}fh + \xi_H^f\bar{f}fH - i\xi_A^f\bar{f}\gamma_5 fA) \\ &+\left[\frac{\sqrt{2}V_{ud}}{v}\bar{u}(m_u\xi_A^u P_L + m_d\xi_A^d P_R)dH^+ \right. \\ &\left. +\frac{\sqrt{2}m_\ell\xi_A^e}{v}\bar{\nu}P_R eH^+ + \text{H.c.}\right],\end{aligned} \tag{14}$$

where $P_{L,R} = (1\mp\gamma_5)/2$, and the factors ξ_ϕ^f ($\phi = h, H$, and A) are listed in Table II. We note that the ξ_h^f and ξ_H^f are rewritten by

$$\begin{aligned}\xi_h^f &= \sin(\beta-\alpha) + 2T_3^f\xi_A^f\cos(\beta-\alpha), \\ \xi_H^f &= \cos(\beta-\alpha) - 2T_3^f\xi_A^f\sin(\beta-\alpha),\end{aligned} \tag{15}$$

where $T_3^f = 1/2(-1/2)$ for $f = u$ (d, e).

TABLE II. The mixing factors in each type of Yukawa interaction in the THDMs [40].

	ξ_h^u	ξ_h^d	ξ_h^ℓ	ξ_H^u	ξ_H^d	ξ_H^ℓ	ξ_A^u	ξ_A^d	ξ_A^ℓ
Type-I	$\cos\alpha/\sin\beta$	$\cos\alpha/\sin\beta$	$\cos\alpha/\sin\beta$	$\sin\alpha/\sin\beta$	$\sin\alpha/\sin\beta$	$\sin\alpha/\sin\beta$	$\cot\beta$	$-\cot\beta$	$-\cot\beta$
Type-II	$\cos\alpha/\sin\beta$	$-\sin\alpha/\cos\beta$	$-\sin\alpha/\cos\beta$	$\sin\alpha/\sin\beta$	$\cos\alpha/\cos\beta$	$\cos\alpha/\cos\beta$	$\cot\beta$	$\tan\beta$	$\tan\beta$
Type-X	$\cos\alpha/\sin\beta$	$\cos\alpha/\sin\beta$	$-\sin\alpha/\cos\beta$	$\sin\alpha/\sin\beta$	$\sin\alpha/\sin\beta$	$\cos\alpha/\cos\beta$	$\cot\beta$	$-\cot\beta$	$\tan\beta$
Type-Y	$\cos\alpha/\sin\beta$	$-\sin\alpha/\cos\beta$	$\cos\alpha/\sin\beta$	$\sin\alpha/\sin\beta$	$\cos\alpha/\cos\beta$	$\sin\alpha/\sin\beta$	$\cot\beta$	$\tan\beta$	$-\cot\beta$

After taking the same rotation of the scalar bosons given in Eq. (5), the Higgs gauge gauge-type terms are expressed by

$$\mathcal{L}_{\rm kin}^{\phi VV} = [\sin(\beta-\alpha)h + \cos(\beta-\alpha)H] \times \left(\frac{m_W^2}{v} W^{+\mu} W_\mu^- + \frac{1}{2}\frac{m_Z^2}{v} Z^\mu Z_\mu\right). \quad (16)$$

Here, we comment on two important limits: the *SM-like limit* and the *decoupling limit* [65], which are realized by taking $\sin(\beta-\alpha)\to 1$ and $M^2\to\infty$, respectively. In the former limit, as seen in Eqs. (14), (15), and (16), the strength of the Yukawa interaction and the gauge interaction of h become the same as in the SM. We thus define h as the SM-like Higgs boson that should be identified as the discovered Higgs boson with the mass of around 126 GeV, and all the other Higgs bosons, $H^\pm$, A, and H are regarded as the additional Higgs bosons. On the other hand, in the decoupling limit, all the masses of additional Higgs bosons become infinity as long as we take the SM-like limit. As a result, only the mass of h remains at the electroweak scale.

If we consider the case without the SM-like limit, we cannot take the decoupling limit. This can be seen by looking at Eq. (9), which tells us that, in order to keep a fixed nonzero value of $\tan 2(\beta-\alpha)$, we need sizable contributions from M_{11}^2 and M_{12}^2 to cancel a large value of M_{22}^2 by the M^2 term in Eq. (11). However, as seen in Eqs. (10) and (12), M_{11}^2 and M_{12}^2 are given like a form of $\lambda_i v^2$ so that when these terms are too large they make λ coupling constants, which are disfavored by the constraints from perturbative unitarity, too large [67,68]. Therefore, there is an upper limit for the mass of additional Higgs bosons at which we retain the deviation from the SM-like limit.

B. Vacuum stability and unitarity

To keep a stability of the vacuum, the Higgs potential should be bounded from below in any directions with a large value of scalar fields. The sufficient condition is given by [69,70]

$$\lambda_1 > 0, \qquad \lambda_2 > 0,$$
$$\sqrt{\lambda_1\lambda_2} + \lambda_3 + \mathrm{MIN}(0, \lambda_4+\lambda_5, \lambda_4-\lambda_5) > 0. \quad (17)$$

In addition, the magnitude of several combinations of the quartic Higgs coupling constants are constrained by unitarity. When we consider the elastic scatterings of two-body boson states, there are 14 neutral, 8 singly charged, and 3 doubly charged channels. After the diagonalization of the T matrix for the S-wave amplitude of these processes, we obtain the 12 independent eigenvalues [68] as

$$x_1^\pm = \frac{1}{32\pi}[3(\lambda_1+\lambda_2) \pm \sqrt{9(\lambda_1-\lambda_2)^2 + 4(2\lambda_3+\lambda_4)^2}], \quad (18)$$

$$x_2^\pm = \frac{1}{32\pi}\left[(\lambda_1+\lambda_2) \pm \sqrt{(\lambda_1-\lambda_2)^2 + 4\lambda_4^2}\right], \quad (19)$$

$$x_3^\pm = \frac{1}{32\pi}\left[(\lambda_1+\lambda_2) \pm \sqrt{(\lambda_1-\lambda_2)^2 + 4\lambda_5^2}\right], \quad (20)$$

$$x_4^\pm = \frac{1}{16\pi}(\lambda_3 + 2\lambda_4 \pm 3\lambda_5), \quad (21)$$

$$x_5^\pm = \frac{1}{16\pi}(\lambda_3 \pm \lambda_4), \quad (22)$$

$$x_6^\pm = \frac{1}{16\pi}(\lambda_3 \pm \lambda_5). \quad (23)$$

For each eigenvalue, we impose the following criterion[7]:

$$|x_i^\pm| \le \frac{1}{2}. \quad (24)$$

As we mentioned in the previous subsection, the unitarity and vacuum stability bounds can be used to obtain the upper limit on the mass of additional Higgs bosons when $\sin(\beta-\alpha)$ deviates from unity. We introduce the scaling factor κ_V defined by the ratio of the hVV coupling constant to the corresponding SM value, which coincides with $\sin(\beta-\alpha)$ at the tree level. In Fig. 1, we show the upper limit of m_A from the unitarity and vacuum stability bounds for given values of $1-\kappa_V$ and $\tan\beta$. The value of M is scanned over the range of $m_A \pm 500$ GeV. To avoid the constraint from the rho parameter, we take $m_{H^+} = m_A$ in these plots so that the one-loop corrections to the rho parameter from the additional Higgs boson loops become zero due to the custodial symmetry in the Higgs potential [29–35]. The value of m_H is taken to be the same as m_A (scanned over the range of $m_A \pm 500$ GeV) in the solid (dotted) curves. The left and right panels show the cases with $\cos(\beta-\alpha) > 0$ and $\cos(\beta-\alpha) < 0$, respectively. It is seen that the maximal allowed value of m_A gets larger when the deviation in κ_V from unity gets small. Therefore, larger deviations in the hVV coupling constant give a severe upper bound on masses for additional Higgs bosons.

In Fig. 2, we show the $\tan\beta$ dependence of the upper limit of m_A from the unitarity and vacuum stability bounds for a given value of $1-\kappa_V$. The other parameters are taken to be the same as in Fig. 1.

C. Decay of the Higgs bosons

In this subsection, we discuss the decays of Higgs bosons with the four types of Yukawa interaction in the THDM. The decay property can be drastically different between the case with $\sin(\beta-\alpha)=1$ and that with $\sin(\beta-\alpha)\neq 1$ [40]. When the SM-like limit is taken, the additional Higgs

[7]Constraints on the parameter space using scale-dependent coupling constants were studied in the THDM in Refs. [70,71].

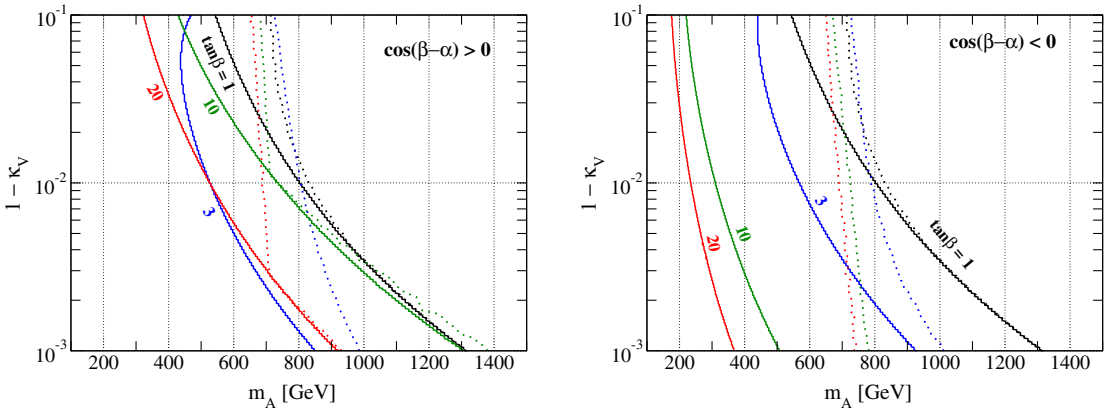

FIG. 1 (color online). Upper limit of $1-\kappa_V$ as a function of m_A for each value of $\tan\beta$ from the constraints of unitarity and vacuum stability in the case in which M is scanned over the range of $m_A \pm 500$ GeV and $m_{H^+} = m_A$. The left and right panels, respectively, show the results with $\cos(\beta-\alpha) > 0$ and $\cos(\beta-\alpha) < 0$. The solid curves show the case with $m_H = m_A$, while the dotted curves show the result with m_H to be scanned over the range of $m_A \pm 500$ GeV.

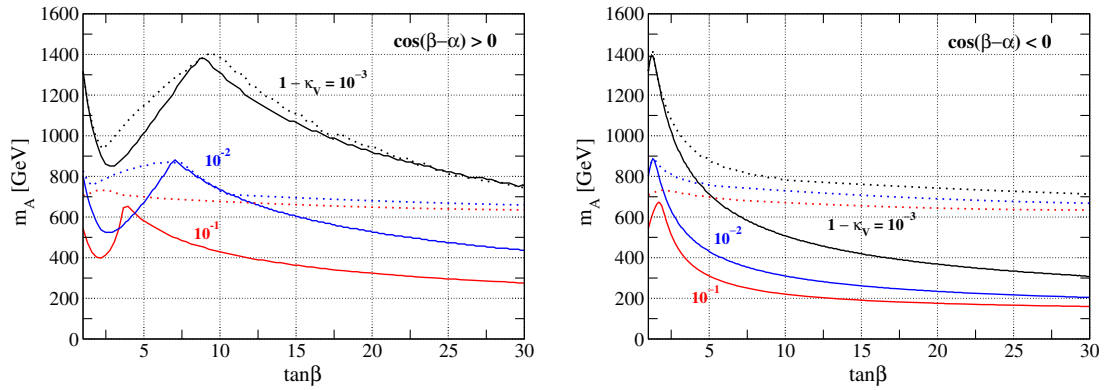

FIG. 2 (color online). Upper limit of m_A as a function of $\tan\beta$ for each value of $1-\kappa_V$ from the constraints of unitarity and vacuum stability in the case in which M is scanned over the range of $m_A \pm 500$ GeV and $m_{H^+} = m_A$. The left and right panels, respectively, show the results with $\cos(\beta-\alpha) > 0$ and $\cos(\beta-\alpha) < 0$. The solid curves show the result with $m_H = m_A$, while the dotted curves show the result with m_H to be scanned over the range of $m_A \pm 500$ GeV.

bosons can dominantly decay into a fermion pair for which the decay branching ratio strongly depends on the type of Yukawa interactions and $\tan\beta$. On the other hand, when we take $\sin(\beta-\alpha) \neq 1$, H can decay into the gauge boson pairs W^+W^- and ZZ and the SM-like Higgs boson pair hh, where these decay rates are proportional to $\cos^2(\beta-\alpha)$. At the same time, $H^\pm$ and A can decay into $W^\pm$ and Z associated with the SM-like Higgs boson h for which the decay amplitudes are also proportional to $\cos(\beta-\alpha)$ [53–55,72].

To calculate the decay rates, we use the following inputs from the Particle Data Group (PDG) [20]:

$$\begin{aligned} &m_Z = 91.1876\ \text{GeV}, \quad m_W = 80.385\ \text{GeV}, \\ &G_F = 1.1663787 \times 10^{-5}\ \text{GeV}^{-2}, \quad m_t = 173.07\ \text{GeV}, \\ &\alpha_s(m_Z) = 0.1185, \quad V_{cb} = 0.0409, \quad V_{ts} = 0.0429. \end{aligned} \tag{25}$$

The running quark masses at the scale of m_Z are quoted from Ref. [73] as

$$\begin{aligned} &\bar{m}_b = 3.0\ \text{GeV}, \qquad \bar{m}_c = 0.677\ \text{GeV}, \\ &\bar{m}_s = 0.0934\ \text{GeV}. \end{aligned} \tag{26}$$

The mass of the SM-like Higgs boson h is taken to be 126 GeV in the following calculations.

All the other parameters shown in Eq. (25) are quoted from the PDG [20]. We note that the effects of Cabibbo-Kobayashi-Maskawa matrix elements V_{cb} and V_{ts} appear in the $H^\pm \to cb$ and $H^\pm \to ts$ decays. For simplicity, we take all the masses of additional Higgs bosons to be the same; i.e., $m_{H^+} = m_A = m_H (\equiv m_\Phi)$. In that case, there are four free parameters in the Higgs potential, which are chosen as m_Φ, M^2, $\tan\beta$, and $\sin(\beta-\alpha)$.

We here comment on the $H^\pm \to W^\pm Z$ and $H^\pm \to W^\pm\gamma$ processes. The $H^\pm W^\mp \gamma$ vertex is obtained at the one-loop

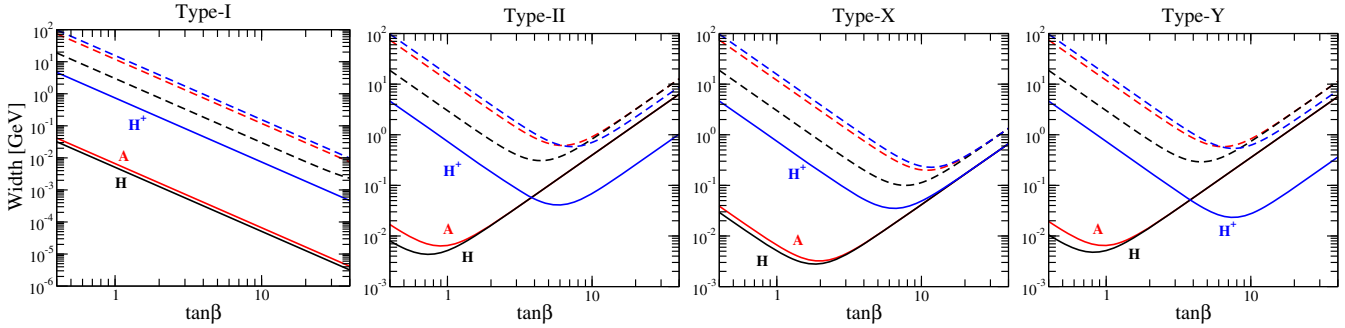

FIG. 3 (color online). Total widths for H, A, and $H^{\pm}$ as a function of $\tan\beta$ in the case of $\sin(\beta-\alpha)=1$. The solid and dashed curves, respectively, show the results with $m_{\Phi}=M=200$ GeV and $m_{\Phi}=M=400$ GeV.

level, and its magnitude is suppressed due to the $U(1)_{\rm em}$ gauge invariance. This nature does not depend on a model. On the other hand, in the THDM, although the $H^{\pm}W^{\mp}Z$ vertex appears at the one-loop level, it can enhance if there is a large violation of the custodial symmetry. As we discussed in the Introduction, the mass splitting between the top and bottom quarks breaks the custodial symmetry, and it gives the $(m_t-m_b)^2$ dependence in the one-loop corrected rho parameter. A similar effect appears in the $H^{\pm}W^{\mp}Z$ vertex [74]. In addition, when the mass splitting

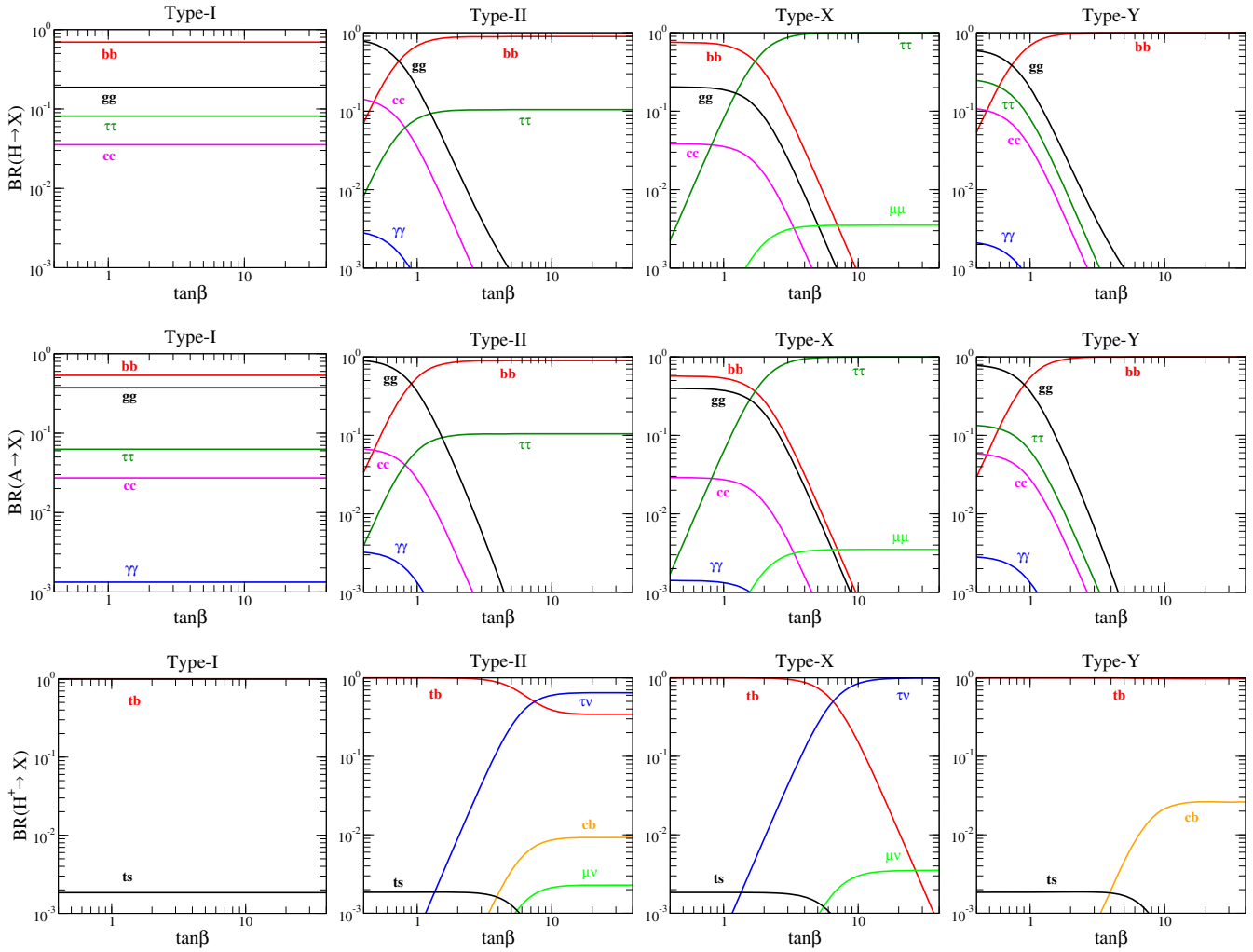

FIG. 4 (color online). Decay branching ratios for H, A, and $H^{\pm}$ as a function of $\tan\beta$ in the case of $m_{\Phi}=M=200$ GeV and $\sin(\beta-\alpha)=1$.

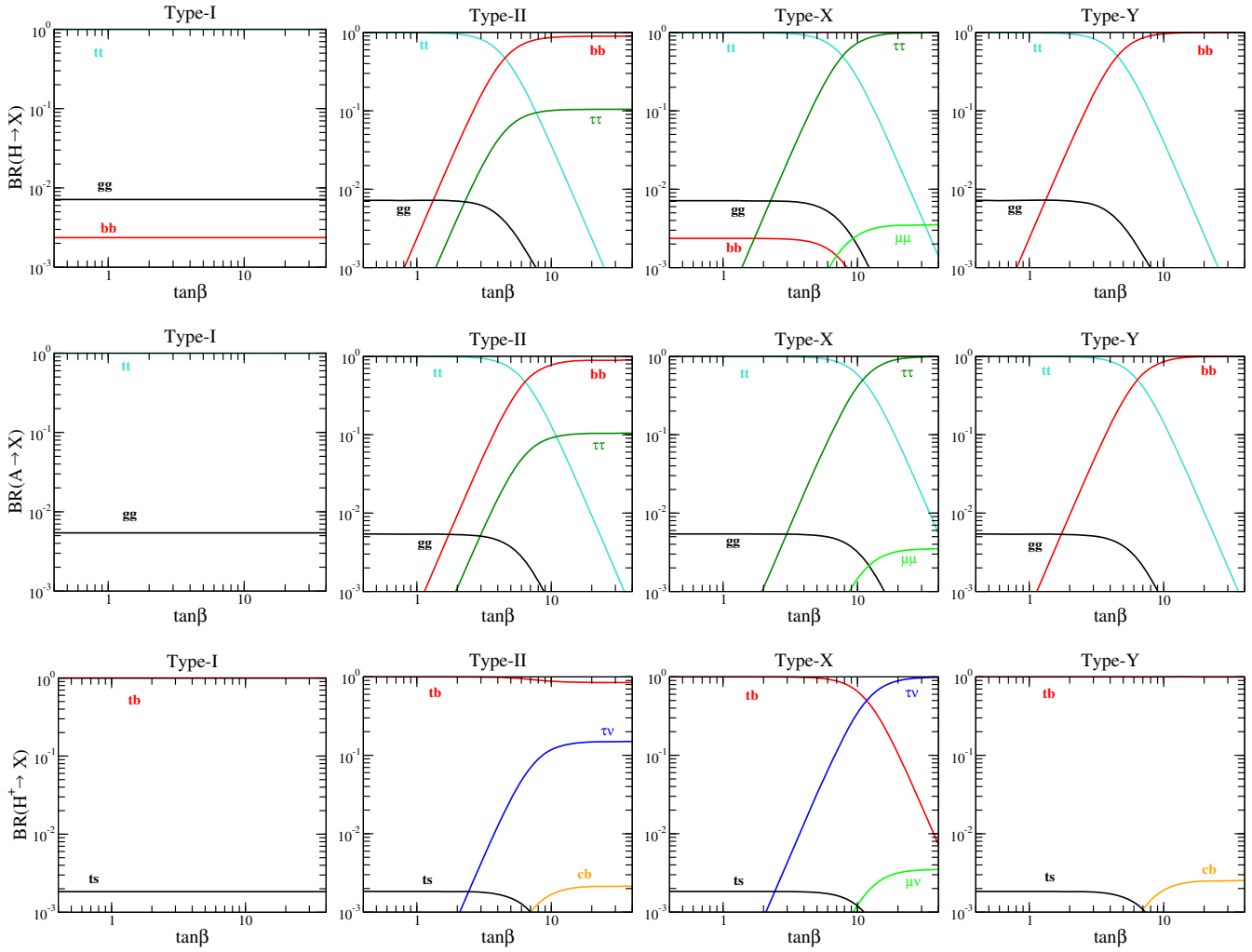

FIG. 5 (color online). Decay branching ratios for H, A, and $H^{\pm}$ as a function of $\tan\beta$ in the case of $m_{\Phi} = M = 400$ GeV and $\sin(\beta - \alpha) = 1$.

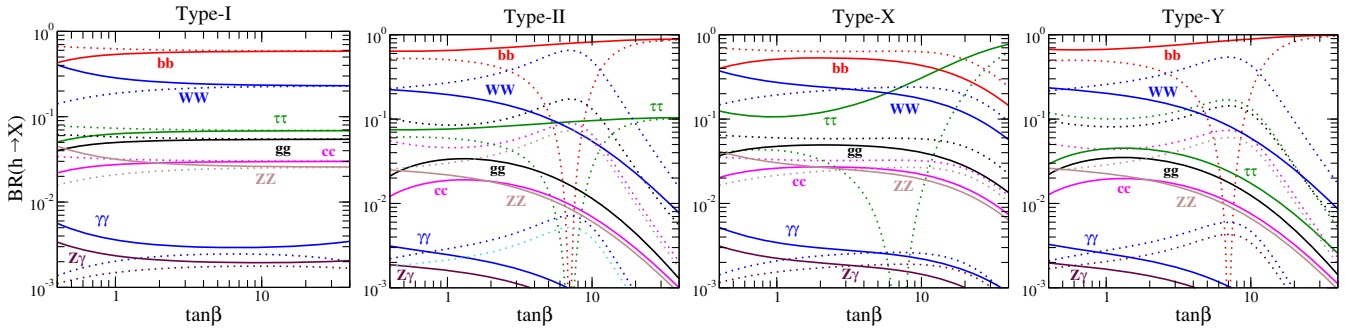

FIG. 6 (color online). Decay branching ratios for h as a function of $\tan\beta$ in the case of $m_{\Phi} = M = 200$ GeV and $\sin(\beta - \alpha) = 0.99$. The solid and dashed curves respectively show the cases with $\cos(\beta - \alpha) < 0$ and $\cos(\beta - \alpha) > 0$.

between $H^{\pm}$ and A is given, which breaks the custodial symmetry in the Higgs potential, the $H^{\pm}W^{\mp}Z$ vertex can be enhanced due to the $(m_{H^+} - m_A)^2$ dependence. In Ref. [75], full one-loop calculation of the $H^{\pm}W^{\mp}Z$ vertex was done. It was shown that the branching ratio of $H^{\pm} \to W^{\pm}Z$ can be $\mathcal{O}(10^{-2})$ in the case of $m_{H^+} = 300$ GeV when the mass splitting between $H^{\pm}$ and A is taken to be $\mathcal{O}(100)$ GeV. In the following calculation, we assume $m_{H^+} = m_A$ so that only the top and bottom quarks loop contribution to the $H^{\pm} \to W^{\pm}Z$ vertex is important. In this

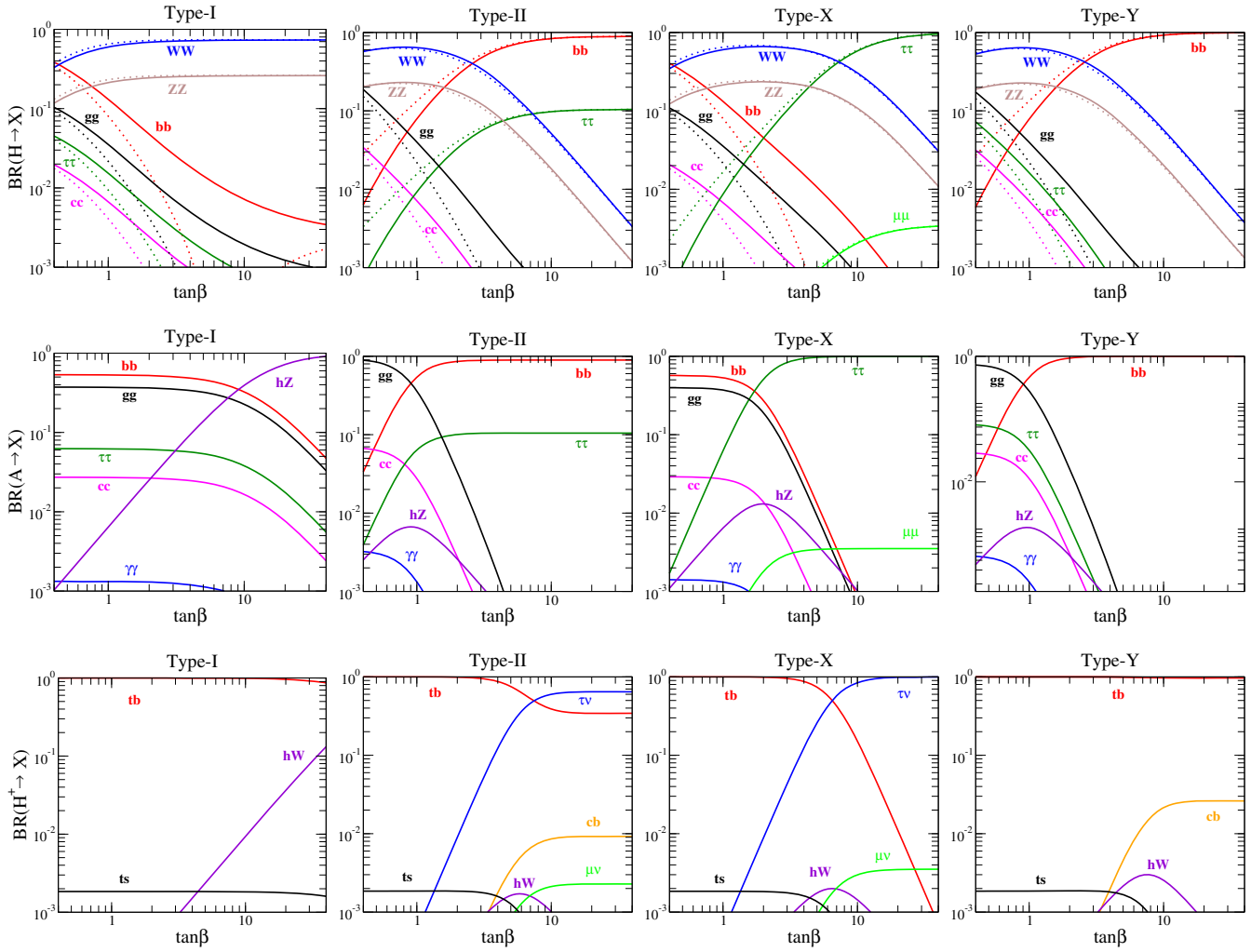

FIG. 7 (color online). Decay branching ratios for H, A, and $H^{\pm}$ as a function of $\tan\beta$ in the case of $m_{\Phi} = M = 200$ GeV and $\sin(\beta-\alpha) = 0.99$. For the H decay, the solid and dashed curves, respectively, show the cases with $\cos(\beta-\alpha) < 0$ and $\cos(\beta-\alpha) > 0$.

case, typical values of the branching fractions of $H^{\pm} \to W^{\pm}Z$ and $H^{\pm} \to W^{\pm}\gamma$ are smaller than $\mathcal{O}(10^{-3})$ and $\mathcal{O}(10^{-5})$, respectively.[8] We thus safely neglect these modes in the following calculation.

First, we show the total widths for H, A, and $H^{\pm}$ in Fig. 3 as a function of $\tan\beta$ in the case of $\sin(\beta-\alpha) = 1$. The solid (dashed) curves show the results with $m_{\Phi} = M = 200(400)$ GeV. Except in the type-I THDM, the widths have a minimum in a certain value of $\tan\beta$ because the sum of the decay rates of the fermion pair mode are given by terms proportional to $\cot^2\beta$, $\tan^2\beta$ and those without $\tan\beta$ dependence. In the type-I THDM, all the decay rates with the fermion pair final state are suppressed by $\cot^2\beta$ so that the widths monotonously decrease when $\tan\beta$ gets larger values. In the type-X THDM, all the widths for H, A and $H^{\pm}$ approach roughly the same value in the high $\tan\beta$ region for a fixed value of m_{Φ}. This can be understood in such a way that the decay rate of $H^{\pm} \to tb$ mainly deviates the width of $H^{\pm}$ from that of H and A, which can be neglected in the high $\tan\beta$ region in the type-X THDM. In the type-I THDM, although the decay rate of $H^{\pm} \to tb$ is suppressed as in the type-X THDM, all the other fermion pair decay modes are also suppressed at the same time. Therefore, the $H^{\pm} \to tb$ decay is not negligible in the type-I THDM, and then it deviates the width of $H^{\pm}$ from that of H and A.

In Fig. 4, we show the decay branching fractions of H (top panels), A (middle panels), and $H^{\pm}$ (bottom panels) as a function of $\tan\beta$ in the case of $\sin(\beta-\alpha) = 1$ and $m_{\Phi} = M = 200$ GeV. It is seen that only in the type-X THDM H and A can mainly decay into $\tau^+\tau^-$ in the case of

[8] If the Higgs sector contains *exotic* Higgs fields for which the isospin is larger than $1/2$, the $H^{\pm}W^{\mp}Z$ vertex appears at the tree level [76]. The magnitude depends on VEVs from exotic Higgs fields that are usually severely constrained by the rho parameter. In the GM model and in the doublet-septet model, such a VEV can be taken as $\mathcal{O}(10)$ GeV. Therefore, measuring the $H^{\pm}W^{\mp}Z$ vertex can be a probe of exotic Higgs sectors. The feasibility study for the measurement of the vertex was performed in Ref. [77] at the LHC and in Ref. [78] at the ILC.

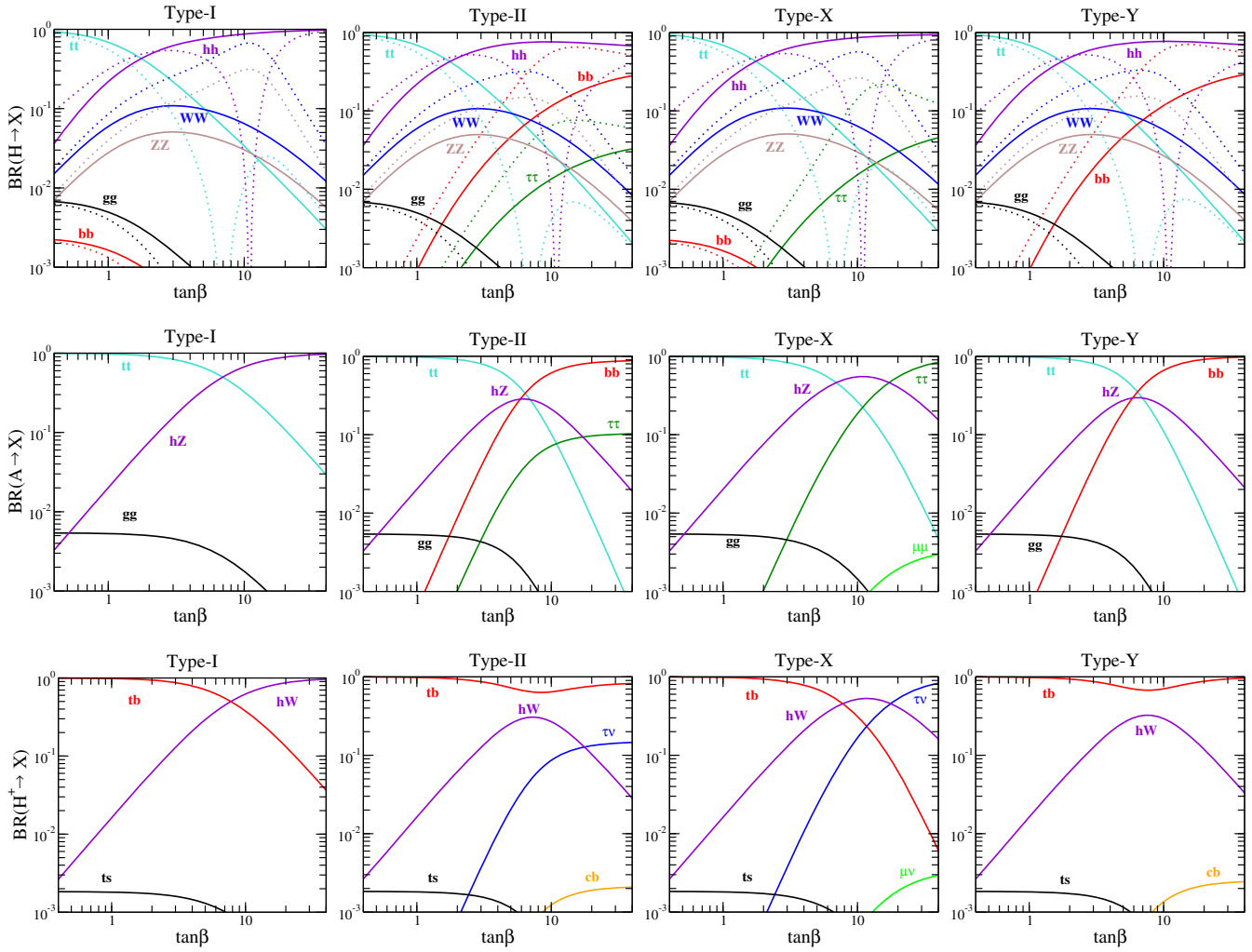

FIG. 8 (color online). Decay branching ratios for H, A, and $H^{\pm}$ as a function of $\tan\beta$ in the case of $m_{\Phi} = M = 400$ GeV and $\sin(\beta-\alpha) = 0.99$. For the H decay, the solid and dashed curves, respectively, show the cases with $\cos(\beta-\alpha) < 0$ and $\cos(\beta-\alpha) > 0$.

$\tan\beta \gtrsim 3$. Besides, H and A can also decay into $\mu^+\mu^-$ with about 0.3% in the type-X THDM. Regarding the $H^{\pm}$ decay, although the main decay mode is basically tb in all the types, that is replaced by $H^{\pm} \to \tau^{\pm}\nu$ in the type-II and type-X THDMs with $\tan\beta \gtrsim 7$.

Similarly, Fig. 5 shows the branching fractions of H, A, and $H^{\pm}$ in the case of $m_{\Phi} = M = 400$ GeV and $\sin(\beta-\alpha) = 1$. In all the types of THDMs, H and A mainly decay into the top pair in the lower $\tan\beta$ region. However, that is replaced by $b\bar{b}$ ($\tau^+\tau^-$) in the type-II and type-Y (type-X) THDMs with $\tan\beta \gtrsim 5$ ($\tan\beta \gtrsim 8$). The decay of $H^{\pm}$ does not change so much from that in the case of $m_{\Phi} = M = 200$ GeV. Notice here that the magnitude relation between the branching fraction of $H/A \to gg$ and that of $H/A \to b\bar{b}$ is flipped compared to the results in Fig. 4 except in the type-II and type-Y THDMs with $\tan\beta \gtrsim 1$. We note that, in the case of $\sin(\beta-\alpha) = 1$ and $m_H = m_A$, only the difference between the decay rate of $H \to f\bar{f}$ and that of $A \to f\bar{f}$ appears in the power of the phase space factor; i.e., that is the cubic (linear) power for H (A) [9]. Thus, the decay rate of $A \to f\bar{f}$ is slightly larger than that of $H \to f\bar{f}$. Moreover, the decay rates of loop-induced modes such as the decays into gg, $\gamma\gamma$, and $Z\gamma$ are different between H and A because of the CP property.

Next, we show the branching fractions in the case without taking the SM-like limit, e.g., $\sin(\beta-\alpha) = 0.99$. In this case, the sign of $\cos(\beta-\alpha)$ can affect decay properties for the CP-even Higgs bosons so that we consider both the cases with $\cos(\beta-\alpha) < 0$ and $\cos(\beta-\alpha) > 0$.

In Fig. 6, the branching fractions for the SM-like Higgs boson h is shown as a function of $\tan\beta$ in the case of $m_{\Phi} = M = 200$ GeV. For the h decay, the m_{Φ} and M parameters affect the $H^{\pm}$ loop contribution to the decay rates of $h \to \gamma\gamma$ and $h \to Z\gamma$. When we take a larger value of m_{Φ} keeping $m_{\Phi} = M$, the $H^{\pm}$ loop contribution vanishes. The solid and dashed curves, respectively, show the

cases with $\cos(\beta-\alpha)<0$ and $\cos(\beta-\alpha)>0$. We can see that several fermionic decay channels vanish at $\tan\beta\simeq 7$ in the case of $\cos(\beta-\alpha)>0$ in the type-II, type-X, and type-Y THDMs. Let us explain this behavior by introducing δ defined by $\sin(\beta-\alpha)=1-\delta$. When $\delta\ll 1$, the ξ_h^f and ξ_H^f factors in Eq. (15) can be approximately expressed by

$$\xi_h^f \simeq 1+\mathrm{Sign}[\cos(\beta-\alpha)]2\sqrt{2\delta}T_3^f\xi_A^f,$$
$$\xi_H^f \simeq \mathrm{Sign}[\cos(\beta-\alpha)]2\sqrt{2\delta}-2T_3^f\xi_A^f. \quad (27)$$

From Table II, we can obtain $\xi_h^f\simeq 1-\mathrm{Sign}[\cos(\beta-\alpha)]\sqrt{2\delta}\tan\beta$ for $f=b$ $(f=\tau)$ in type-II and type-Y (type-II and type-X) THDMs. Thus, when $\cos(\beta-\alpha)$ is positive, and δ is taken to be 0.01, ξ_h^f becomes zero at around $\tan\beta=7$. We note that the ξ_h^f factor can be -1 in the case of $\cos(\beta-\alpha)<0$, in which the sign of Yukawa coupling constant is opposite compared to the SM value. Signatures of additional Higgs bosons in the parameter regions with $\xi_h^f\simeq -1$ have been studied in Ref. [56], and the testability of the sign of Yukawa couplings has been investigated at a future linear collider in Ref. [57].

The branching fractions for the additional Higgs bosons are also shown in Fig. 7 in the case of $m_\Phi=M=200$ GeV, and those in the case of $m_\Phi=M=400$ GeV are shown in Fig. 8. For the H decay, we use the solid and dashed curves, respectively, to show the cases with $\cos(\beta-\alpha)<0$ and $\cos(\beta-\alpha)>0$. It can be seen that the gaugephobic nature of H is lost, and the $H\to W^+W^-/ZZ$ modes can be dominate. Regarding the A and $H^\pm$ decays, the $A\to hZ$ and $H^\pm\to hW^\pm$ modes are added to the case with $\sin(\beta-\alpha)=1$. When we consider heavier case of H, $m_\Phi=M=400$ GeV, the $H\to hh$ mode for which the decay rate is proportional to $\cos^2(\beta-\alpha)$ is kinematically allowed. This can be the main decay mode as we can see in the top panels in Fig 8.

We comment on the case without degeneracy in mass of the additional Higgs bosons. In that case, heavier additional Higgs bosons can decay into lighter ones associated with a gauge boson even in the SM-like limit. For instance, when $m_H>m_A$, the $H\to AZ^{(*)}$ mode is allowed. Recently, signatures from $H\to AZ$ and $A\to HZ$ decays have been studied at the LHC in Ref. [55].

III. DIRECT SEARCH FOR ADDITIONAL HIGGS BOSONS AT THE LHC

At the LHC with the collision energy of 7 and 8 TeV, so far, there is no report for a discovery of new particles other than a Higgs boson, and only exclusion bounds for masses of hypothetical particles are obtained.

First of all, we review the current bounds on parameter space in the THDMs from 7 and 8 TeV data at the LHC. The signal of neutral Higgs bosons in the $\tau^+\tau^-$ decay mode has been searched for in the inclusive production and bottom quark-associated production processes [10,11]. For the type-II THDM, bounds on $\tan\beta$ have been obtained for given values of m_A, e.g., $\tan\beta\lesssim 10$ for $m_A=300$ GeV and $\tan\beta\lesssim 40$ for $m_A=800$ GeV [11]. In addition, the searches for the $b\bar{b}$ decay of neutral Higgs bosons in the bottom quark-associated process have been performed [12]. The $b\bar{b}$ decay mode gives a rather weaker bound on $\tan\beta$ compared to the $\tau^+\tau^-$ decay mode. These bounds can be used to constrain parameter regions in both the type-II and type-Y THDMs. Furthermore, for $\sin(\beta-\alpha)<1$, searches for the $H\to W^+W^-$ signal have been performed [13], and a bound on the m_H-$\cos\alpha$ plane is obtained for given values of $\tan\beta$. This bound is not sensitive to the type of Yukawa interaction. In Ref. [14], $H\to hh$ and $A\to Zh$ decays have been searched, and bounds on the cross section times branching ratio have been obtained. These can be translated into the exclusion regions in the $\cos(\beta-\alpha)$-$\tan\beta$ plane for given values of $m_{H/A}$ for each type of Yukawa interaction.

In the following, we discuss expected excluded regions on the m_A-$\tan\beta$ plane at the LHC with the collision energy of 14 TeV. We first focus on the search for H and A by using the tau decay from the gluon fusion and bottom quark-associated production processes as

$$gg\to\phi^0\to\tau^+\tau^-, \quad (28)$$

$$gg\to b\bar{b}\phi^0\to b\bar{b}\tau^+\tau^-, \quad (29)$$

where $\phi^0=H$ or A. The cross sections for the above processes can be estimated by[9]

$$\sigma(gg\to\phi^0)=\frac{\Gamma(\phi^0\to gg)}{\Gamma(h_{\rm SM}\to gg)_{m_{\phi^0}}}\sigma(gg\to h_{\rm SM})_{m_{\phi^0}}, \quad (30)$$

$$\sigma(gg\to b\bar{b}\phi^0)=(\xi_d^{\phi^0})^2\sigma(gg\to b\bar{b}h_{\rm SM})_{m_{\phi^0}}, \quad (31)$$

where $h_{\rm SM}$ is the SM Higgs boson. In Eq. (30), $\Gamma(h_{\rm SM}\to gg)_{m_{\phi^0}}$ and $\sigma(gg\to h_{\rm SM})_{m_{\phi^0}}$ are, respectively, the decay rate of $h_{\rm SM}\to gg$ and the cross section of the gluon fusion process by taking the mass of $h_{\rm SM}$ to be replaced by the mass of ϕ^0 (m_{ϕ^0}). We use the values of the gluon fusion cross section in the SM at 14 TeV from Ref. [79]. In Eq. (31), $\sigma(gg\to b\bar{b}h_{\rm SM})_{m_{\phi^0}}$ is the cross section for the bottom quark-associated production of $h_{\rm SM}$ with the mass of $h_{\rm SM}$ to be replaced by m_{ϕ^0}. We calculate $\sigma(gg\to b\bar{b}h_{\rm SM})_{m_{\phi^0}}$ by using CalcHEP [80] with CTEQ6L [81] for the parton distribution functions (PDFs).

The signal and background analyses for these processes have been done in the MSSM in Refs. [82,83]. The signal significances for the processes expressed in Eqs. (30) and

[9]Regarding Eq. (31), the equation for $\phi^0=A$ holds when the bottom quark mass in the phase space function is neglected.

(31) are given in the case of $\tan\beta = 10$ and several fixed masses of A with the collision energy of 14 TeV and the integrated luminosity of 30 fb^{-1}. In Table III, the significance for each fixed value of m_A is listed, where $\mathcal{S}^{\phi^0}_{\rm MSSM}$ and $\mathcal{S}^{b\bar{b}\phi^0}_{\rm MSSM}$ are, respectively, the significances for the gluon fusion process and the bottom quark-associated process. These significances evaluated in the MSSM can be converted into those in the THDMs by using the equations

$$\mathcal{S}^{\phi^0}_{\rm THDM} = \mathcal{S}^{\phi^0}_{\rm MSSM} \times \frac{\sum_{\phi^0=H,A}\sigma(gg\to\phi^0)\times\mathcal{B}(\phi^0\to\tau^+\tau^-)|_{\rm THDM}}{\sum_{\phi^0=H,A}\sigma(gg\to\phi^0)\times\mathcal{B}(\phi^0\to\tau^+\tau^-)|_{\rm MSSM}} \times \sqrt{\frac{\mathcal{L}}{30\ {\rm fb}^{-1}}}, \tag{32}$$

$$\mathcal{S}^{b\bar{b}\phi^0}_{\rm THDM} = \mathcal{S}^{b\bar{b}\phi^0}_{\rm MSSM} \times \frac{\sum_{\phi^0=H,A}\sigma(gg\to b\bar{b}\phi^0)\times\mathcal{B}(\phi^0\to\tau^+\tau^-)|_{\rm THDM}}{\sum_{\phi^0=H,A}\sigma(gg\to b\bar{b}\phi^0)\times\mathcal{B}(\phi^0\to\tau^+\tau^-)|_{\rm MSSM}} \times \sqrt{\frac{\mathcal{L}}{30\ {\rm fb}^{-1}}}, \tag{33}$$

where $\mathcal{L}$ is the assumed integrated luminosity. In the above expression, when m_{ϕ^0} is taken in the range of $X \le m_{\phi^0} \le Y$, where X and Y are values of m_A listed in Table III, we use the values of $\mathcal{S}^{\phi^0}_{\rm MSSM}$ and $\mathcal{S}^{b\bar{b}\phi^0}_{\rm MSSM}$ given in the case with $m_A = X$. The combined significance is calculated by

$$\mathcal{S}_{\rm comb} = \sqrt{(\mathcal{S}^{\phi^0}_{\rm THDM})^2 + (\mathcal{S}^{b\bar{b}\phi^0}_{\rm THDM})^2}, \tag{34}$$

and the expected excluded region with the 95% C.L. is obtained by requiring $\mathcal{S}_{\rm comb} \ge 2$. In the following analysis, we assume $m_A = m_H$ and $\sin(\beta-\alpha) = 1$, and we sum over the processes in Eqs. (30) and (31) mediated by H and A. These assumptions are valid as long as we consider the case with $m_A \gtrsim 150$ GeV, because in the MSSM, $m_H \simeq m_A$ and $\sin(\beta-\alpha) \simeq 1$ are the good approximations in that case.

In Fig. 9, we show the expected excluded regions by using Eq. (34) in the type-II (left panel) and type-X (right panel) THDMs. The blue and red shaded regions are, respectively, the excluded regions assuming $\mathcal{L}$ to be 300 fb^{-1} and 3000 fb^{-1}. In the type-II THDM, the exclusion reach of m_A increases when a larger value of $\tan\beta$ is taken because the cross sections of the bottom quark-associated processes are enhanced due to the coefficient $\xi^b_H = \xi^b_A = \tan\beta$, and the branching fraction of $\phi^0 \to \tau^+\tau^-$ is approaching 10% in high $\tan\beta$ regions as shown in Figs. 4 and 5. On the other hand, in the type-X THDM, both the gluon fusion and the bottom quark-associated production cross sections are suppressed by $\cot^2\beta$ as $\tan\beta$ gets larger, while the branching fraction of $\phi^0 \to \tau^+\tau^-$ increases. Consequently, the cross section times branching ratio takes the maximal obtained at $\tan\beta \simeq 12$, and then $m_A \simeq 600$ GeV can be excluded assuming $\mathcal{L} = 3000$ fb^{-1}. When $\mathcal{L} = 300$ fb^{-1} is assumed, the excluded reach is settled to be 500 GeV in the region of $6 \lesssim \tan\beta \lesssim 20$ in spite of the fact that the cross section has the maximal value at around $\tan\beta = 12$. This can be understood in such a way that the quoted significance $\mathcal{S}^{\phi^0}_{\rm MSSM}$ given in Table III is changed at $m_A = 500$ GeV, and the combined significance $\mathcal{S}_{\rm comb}$ defined in Eq. (34) cannot exceed 2 even in the case with $\tan\beta \simeq 12$. This behavior should vanish by the detailed background analysis with smaller intervals of m_A.

TABLE III. Significance for the gluon fusion process $\mathcal{S}^{\phi^0}_{\rm MSSM}$ and the bottom quark-associated process $\mathcal{S}^{b\bar{b}\phi^0}_{\rm MSSM}$ in the MSSM with $\tan\beta = 10$ at the LHC with the collision energy of 14 TeV and the integrated luminosity of 30 fb^{-1} quoted from Refs. [82,83].

m_A (GeV)	150	200	300	400	450	500
$\mathcal{S}^{\phi^0}_{\rm MSSM}$ [83]	5.6	5.8	1.7	1.1		0.2
$\mathcal{S}^{b\bar{b}\phi^0}_{\rm MSSM}$ [82]	8.0		2.1		1.1	

This result is the updated version of Fig. 1.20 in the ILC Higgs White Paper [51]. In the previous figure, the excluded regions have been derived by using only one value of the significance for the gluon fusion and bottom quark-associated processes with $m_A = 150$ GeV from Ref. [82]. In the current version, we use several values of the significance as shown in Table III.

If we take $\sin(\beta-\alpha) \neq 1$, the contribution from H (A) can drastically decrease because the branching fraction of the $H(A) \to \tau^+\tau^-$ mode significantly decreases due to the $H \to VV$ and $H \to hh$ $(A \to hZ)$ modes as seen in Fig. 6. In such a case, the $H \to ZZ \to 4\ell$ and $A \to hZ \to b\bar{b}\ell\ell$ channels can be important instead of the $\tau^+\tau^-$ mode. In fact, these searches have been studied with the LHC data [4,14]. The performance of the HL-LHC has also been evaluated in Refs. [49]. These results show that masses of $\sim$1 TeV could be explored for $1-\kappa_V \gtrsim 10^{-2}$ with low $\tan\beta \lesssim 3$ [49]. Thus, the parameter space allowed by theoretical consistencies can be fully probed by future LHC data for $1-\kappa_V \gtrsim 10^{-2}$.

Next, we consider the Drell-Yan production;

$$pp \to Z^* \to HA. \tag{35}$$

For given values of the masses for H and A, this cross section is purely determined by the gauge coupling constant so that the cross section does not depend on the type

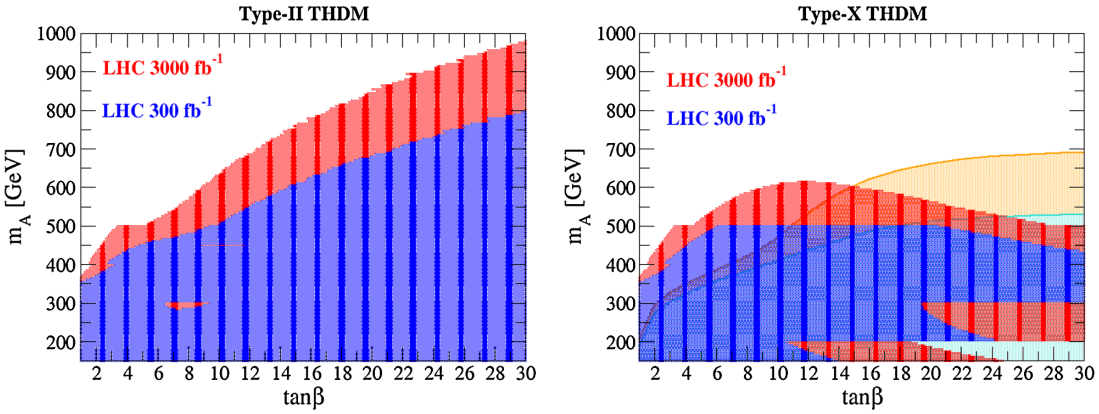

FIG. 9 (color online). Expected excluded regions on the $\tan\beta$-m_A plane at the 95% C.L. from the $gg \to \phi^0 \to \tau^+\tau^-$ and $gg \to b\bar{b}\phi^0 \to b\bar{b}\tau^+\tau^-$ processes by using Eqs. (33) and (34) in the case of $m_A = m_H$ and $\sin(\beta-\alpha) = 1$. The left and right panels show the results in the type-II and type-X THDMs, respectively. The blue (red) shaded regions are excluded regions assuming the integrated luminosity to be 300 fb^{-1} (3000 fb^{-1}). In the right panel, the constraint from the $q\bar{q} \to HA \to \tau^+\tau^-\tau^+\tau^-$ processes is also shown by the light colored regions in the type-X THDM.

of Yukawa interactions. When both H and A decay into the tau pairs, the 4-τ final state is obtained. The cross section of the 4τ process can be large in the type-X THDM as compared to the other three types of THDMs due to the enhancement of the branching fraction of $H/A \to \tau^+\tau^-$ for large $\tan\beta$ [40]. We thus focus on the 4τ signature from the HA production to test the type-X THDM in the following. Analyses on the $pp \to HH^\pm$ and $AH^\pm$ resulting the 3τ signature have been studied in Ref. [84], where the same order bounds on $m_{H^\pm}$ can be obtained.

We estimate the cross section by using the leading-order expression with the CTEQ6L PDFs [81], where the scale of them is set to $\mu = m_H$. The event rates of the $HA \to 4\tau$ signal are obtained by multiplying the production cross section by the branching ratios of H and A into $\tau^+\tau^-$. Furthermore, by using the kinematical distributions of the decay products of τ's that are calculated by PYTHIA [85] and TAUOLA [86], we estimate the efficiency of detecting the signal events after the acceptance and kinematical cuts given in Ref. [84] for all the final states leading from the decays of the four τ's, such as four τ jets, three τ jets plus one lepton, etc. The significance for detecting the $HA \to 4\tau$ process is estimated for a given value of the integrated luminosity, by combining the significance of all the channels in which each significance is evaluated as $S = \sqrt{2[(s+b)\ln(1+s/b) - s]}$ with s and b being the expected numbers of the signal and background events after the cuts, respectively.

In the right panel of Fig. 9, the expected exclusion regions are shown on the $\tan\beta$-m_A plane in the type-X THDM from the $pp \to HA \to 4\tau$ process. The cyan and orange shaded regions are excluded at the 95% C.L. assuming the integrated luminosity to be 300 fb^{-1} and 3000 fb^{-1}, respectively. The search potential is significantly improved for the large $\tan\beta$ regions due to the enhancement of the decay branching ratios of H and A into the $\tau^+\tau^-$ final state. For $\tan\beta \gtrsim 20$, the discovery regions arrive at around $m_A = 500$ GeV for 300 fb^{-1}, while those arrive at around 700 GeV for 3000 fb^{-1}.

We note that the τ-jet tagging efficiency shall worsen at the high-luminosity run of the LHC due to the participation of many hadrons in an event that prevents the isolation requirement in the τ-jet tagging procedure [87]. Therefore, the expected significance may be reduced for the channels with high τ-jet multiplicity, since the τ-jet tagging efficiency used in our analysis is based on the PYTHIA simulation; see Ref. [84]. Although we have not studied this issue seriously, it can be important at the high-luminosity run of the LHC.

In the end of this section, we would like to mention the direct search potential for H and A in the type-I and type-Y THDMs. In the type-I THDM, the Yukawa interactions for the additional Higgs bosons are getting weak for large $\tan\beta$, so it is difficult to generate new bosons via the Yukawa interaction. In type-Y THDM, only the down-type quark Yukawa interactions are enhanced by $\tan\beta$. Since the process $pp \to HX, AH(H, A \to b\bar{b})$ are enhanced for large $\tan\beta$, the cross section times the branching ratio are constrained [12]. The bounds are much weaker than those from $H/A \to \tau^+\tau^-$ decay channels in type-II and type-X THDMs. The analysis with data for high-luminosity running will push these bounds substantially.

Finally, we comment on the constraint from flavor experiments. It is well known that the mass of $H^\pm$ in the type-II THDM is severely constrained by the precise measurements of the $b \to s\gamma$ process [37,38,88,89], where the $H^\pm$ loops contribute to this process in addition to the W boson loop contribution. A lower bound has been found to be $m_{H^+} \gtrsim 380$ GeV (95% C.L.) in the type-II THDM at the next-to-next-to-leading order [89]. In the type-I THDM, the bound from $b \to s\gamma$ is important only in the case with low $\tan\beta$; namely, the bound on m_{H^+} is stronger than the Large Electron

TABLE IV. Expected precisions on the Higgs boson couplings and total width from a constrained seven-parameter fit quoted from Table 1–20 in Ref. [52].

Facility	LHC	HL-LHC	ILC500	ILC500-up	ILC1000	ILC1000-up
$\sqrt{s}$ (GeV)	14,000	14,000	250/500	250/500	250/500/1000	250/500/1000
$\int \mathcal{L}dt$ (fb^{-1})	300/expt	3000/expt	250 + 500	1150 + 1600	250 + 500 + 1000	1150 + 1600 + 2500
κ_γ	5%–7%	2%–5%	8.3%	4.4%	3.8%	2.3%
κ_g	6%–8%	3%–5%	2.0%	1.1%	1.1%	0.67%
κ_W	4%–6%	2%–5%	0.39%	0.21%	0.21%	0.2%
κ_Z	4%–6%	2%–4%	0.49%	0.24%	0.50%	0.3%
κ_ℓ	6%–8%	2%–5%	1.9%	0.98%	1.3%	0.72%
$\kappa_d = \kappa_b$	10%–13%	4%–7%	0.93%	0.60%	0.51%	0.4%
$\kappa_u = \kappa_t$	14%–15%	7%–10%	2.5%	1.3%	1.3%	0.9%

Positron Collider bound of around 80 GeV [20] when $\tan\beta < 2.5$ is taken [89]. The type-Y and type-X THDMs receive similar constraints as in the type-II and type-I THDMs, respectively, because of the same structure of quark Yukawa interactions. Bounds from the other observables such as $B \to \tau\nu$ [90,91], $\tau \to \mu\nu\bar{\nu}$ [91,92], and the muon anomalous magnetic moment [93,94] have been discussed in the type-II THDM. In Ref. [95], constraints from various flavor experiments have been studied in the four types of Yukawa interactions of the THDM. Excluded parameter regions are shown on the m_{H^+}-$\tan\beta$ plane. The bound on m_{H^+} can be converted into that on the masses of neutral Higgs bosons from the electroweak precision data. Although such a constraint can be stronger than that from the direct search as shown in Fig. 9, it is important to search for additional Higgs bosons independently on the flavor experiments.

IV. PRECISION MEASUREMENTS FOR THE HIGGS BOSON COUPLINGS AND FINGERPRINTING EXTENDED HIGGS MODELS

In this section, we discuss the deviation in the SM-like Higgs boson couplings in the THDMs and also in the other models with universal Yukawa couplings. In a model with extended Higgs sectors, the Higgs boson couplings can deviate from the SM values as we already have discussed in Sec. II in the THDMs as an example. Therefore, extended Higgs sectors can be indirectly tested by measuring the deviation of various Higgs boson couplings. Furthermore, the pattern of the deviation strongly depends on the structure of the Higgs sector so that we can discriminate various Higgs sectors by comparing the predicted pattern of the deviations with the measured one.

We here define the scaling factors by normalizing the coupling constant of the SM Higgs boson that will be precisely determined by future collier experiments:

$$\mathcal{L} = \kappa_V h\left(\frac{n_W^2}{v} W^{+\mu} W_\mu^- + \frac{1}{2}\frac{m_Z^2}{v} Z^\mu Z_\mu\right) - \sum_f \kappa_f h \frac{m_f}{v} \bar{f} f. \tag{36}$$

These measured values should be compared with corresponding values in extended Higgs models. In the THDM, κ factors are given at the tree level by

$$\kappa_f = \xi_h^f, \qquad \kappa_V = \sin(\beta - \alpha), \tag{37}$$

where ξ_h^f are listed in Table II. We also discuss the other extended Higgs sectors with universal Yukawa coupling constants; i.e., κ_f for any fermion f are modified in the same way in the end of this section.

The scaling factors will be measured accurately at future collider experiments such as the HL-LHC and the ILC. In Table IV, we give a brief summary of expected sensitivities on the (SM-like) Higgs boson coupling constant at various future experiments. The ranges shown for the LHC and HL-LHC represent the conservative and aggressive scenarios for systematic and theory uncertainties. ILC numbers assume (e^-, e^+) polarizations of $(-0.8, 0.3)$ at 250 and 500 GeV and $(-0.8, 0.2)$ at 1000 GeV, plus a 0.5% theory uncertainty.

A. Higgs boson couplings in the THDMs

We first consider the deviations in the Higgs boson coupling constants in the THDMs. From Table II, it can be seen that all the four types of Yukawa interaction have different combinations of ξ_h^f for $f = u, d$, and e when $\sin(\beta - \alpha) \neq 1$. Therefore, the direction and magnitude of modifications for κ_f are different in four types of Yukawa interactions.

In Figs. 10 and 11, the scaling factors are shown for each type of Yukawa interaction in the THDMs as functions of κ_V^2 and $\tan\beta$. When κ_V^2 is determined, there still is a sign ambiguity for $\cos(\beta - \alpha)$. Thus, we separately plot model predictions for $\cos(\beta - \alpha) < 0$ in Fig. 10 and for $\cos(\beta - \alpha) > 0$ in Fig. 11. Note that the Higgs sector in the MSSM predicts a negative value of $\cos(\beta - \alpha)$. In the left (right) panels, the scaling factors of THDMs are given in the κ_d–κ_ℓ (κ_u–κ_ℓ) plane. Because of the simple scaling in Table II, the predictions in the κ_u–κ_d plane are obtained by interchanging the type-X and type-Y THDMs in the right panels. For illustration purposes only, we slightly shift lines along with

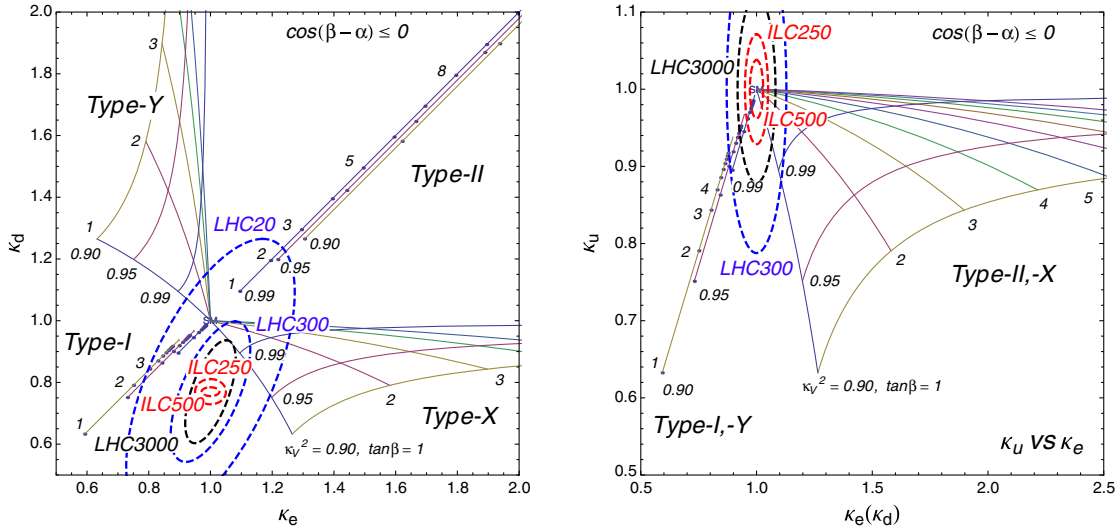

FIG. 10 (color online). The scaling factors for the Yukawa interaction of the SM-like Higgs boson in THDMs in the case of $\cos(\beta-\alpha) < 0$.

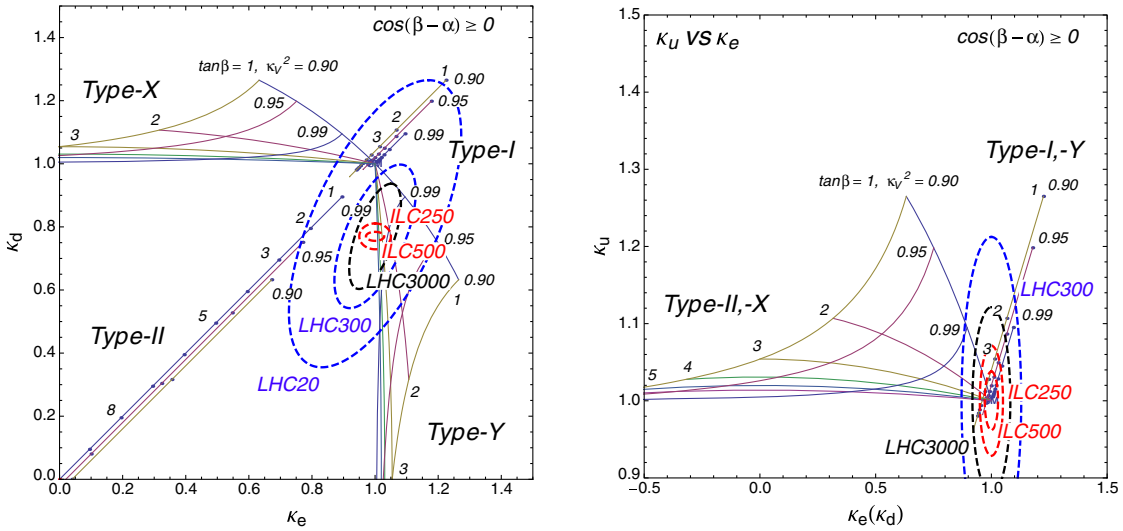

FIG. 11 (color online). The scaling factors for the Yukawa interaction of the SM-like Higgs boson in THDMs in the case of $\cos(\beta-\alpha) > 0$.

$\kappa_x = \kappa_y$ in order to show $\tan\beta$ dependence for fixed κ_V^2 to avoid confusion. The largest contour (LHC20) denotes the current LHC bound at the 68% C.L., where the central values and the correlations are taken from Ref. [64]. We also present the projection at the HL-LHC ($\sqrt{s} = 14$ TeV) with an integrated luminosity of 300 fb^{-1} (LHC300) and 3000 fb^{-1} (LHC3000), where the same central values and the correlations are adopted. The ILC prospects are also shown for ILC250 and ILC500, where the collision energy is 250 GeV and 500 GeV, and the integrated luminosity is 250 fb^{-1} and 500 fb^{-1}, respectively. Each of the THDMs predicts quite a different region, which can be discriminated by the precision measurement of the SM-like Higgs boson coupling constants.

We note that, through the precision measurement of the branching ratios of the SM-like Higgs boson, not only the discrimination of the type of Yukawa interaction but also the determination of $\tan\beta$ in an indirect way can be accomplished [96]. The later complements the determination of $\tan\beta$ by using additional Higgs boson production directly [97].

B. Models with universal Yukawa couplings

We consider Higgs sectors with a universal shift in the Yukawa coupling constants. Such a situation can be realized in a Higgs sector composed of only one doublet field, e.g., a model with a scalar doublet plus singlets,

triplets, and higher isospin multiplets, or in a Higgs sector with multidoublet fields but only one of them giving all the fermion masses, e.g., the type-I THDM. In the following, we first discuss the doublet-singlet model, the type-I THDM, and the doublet-septet model, and then we consider the GM model as models with $\rho_{\text{tree}} = 1$. We note that these extended Higgs sectors can predict larger deviations in the hVV couplings as compared to those in models with $\rho_{\text{tree}} \neq 1$ because an amount of the deviation depends on an additional VEV for which the magnitude is constrained by the rho parameter if it causes $\rho_{\text{tree}} \neq 1$.

In the doublet-singlet model and the soublet-septet model, an isospin singlet field with $Y = 0$ and an isospin septet field with $Y = 2$ are contained, respectively, in addition to the doublet scalar field Φ with $Y = 1/2$. The type-I THDM was already defined in Sec. II. From Eq. (2), a VEV from the additional scalar multiplet does not change ρ_{tree} from the SM value.

Except the VEV of the singlet scalar field, all the VEVs from the additional Higgs multiplet v_{ext} contribute to the electroweak symmetry breaking. They satisfy $v^2 = v_0^2 + (\eta_{\text{ext}} v_{\text{ext}})^2$, where v_0 is the VEV of Φ and $\eta_{\text{ext}} = 1$ and 4 in the type-I THDM and the doublet-septet model, respectively. It is convenient to define the ratio of the VEVs as $\tan\beta = v_0/(\eta_{\text{ext}} v_{\text{ext}})$.

There are two CP-even scalar states in these three models, and they are mixed with the angle α as

$$\begin{pmatrix} h_{\text{ext}} \\ h_0 \end{pmatrix} = R(\alpha) \begin{pmatrix} H \\ h \end{pmatrix}, \tag{38}$$

where h_0 and h_{ext} denote the CP-even scalar components from Φ and an additional scalar multiplet, respectively. The h and H fields are the mass eigenstates, and we assume that h is the observed Higgs boson with the mass of about 126 GeV.

Next, we discuss the GM model for which the Higgs sector is composed of a real ($Y = 0$) and a complex ($Y = 1$) triplet scalar field in addition to Φ. When the VEVs of two triplet fields are aligned to be the same ($= v_{\text{ext}}$), $\rho_{\text{tree}} = 1$ is satisfied, where the contributions to the deviation in ρ_{tree} from unity by the triplet VEVs are cancelled with each other. The value of η_{ext} defined in the above is given as $2\sqrt{2}$.

In the GM model, there are three CP-even scalar states from Φ and two triplets. They are mixed with each other as [98]

$$\begin{pmatrix} \xi_r \\ h_0 \\ \chi_r \end{pmatrix} = \begin{pmatrix} 0 & \frac{1}{\sqrt{3}} & -\sqrt{\frac{2}{3}} \\ 1 & 0 & 0 \\ 0 & \sqrt{\frac{2}{3}} & \frac{1}{\sqrt{3}} \end{pmatrix} \times \begin{pmatrix} \cos\alpha & -\sin\alpha & 0 \\ \sin\alpha & \cos\alpha & 0 \\ 0 & 0 & 1 \end{pmatrix} \begin{pmatrix} H \\ h \\ H_5 \end{pmatrix}, \tag{39}$$

where ξ_r and χ_r are, respectively, the CP-even scalar components in the $Y = 0$ and $Y = 1$ triplet Higgs fields and H_5 is the neutral component of the custodial SU(2) 5-plet Higgs boson.

In Table V, we list the scaling factors κ_f and κ_V in terms of α and β in the four models. In the doublet-singlet model, κ_f and κ_V have the same expression $\cos\alpha$ because both the Yukawa interaction and the gauge interaction originate from the doublet Higgs field, and they are suppressed by the same origin, i.e., the mixing between doublet and singlet fields.

In the type-I THDM, both the Yukawa couplings and the gauge couplings are suppressed by κ_f and κ_V, respectively. However, $\kappa_f \neq \kappa_V$ is generally allowed unlike the doublet-singlet model. We have already mentioned in Sec. II A that we can take the SM-like limit by $\sin(\beta - \alpha) \to 1$, where both κ_f and κ_V become unity. A similar limit can be defined in the doublet-singlet model by taking $\alpha \to 0$.

In the GM model and the doublet-septet model, the VEV of the additional multiplet affects the electroweak symmetry breaking in a different way from that by the doublet Higgs field; i.e., η_{ext} in the GM model and the doublet-septet model are different in the type-I THDM. As a result, κ_V can be larger than 1 (see Table V). This is a unique feature to identify these models. Furthermore, the limit of $\kappa_f \to 1$ and $\kappa_V \to 1$ is taken by setting $\beta = 0$ and $\alpha = -\pi/2$, which corresponds to the special case in the type-I THDM.

In Fig. 12, we show predictions of the scaling factors κ_f and κ_V for each value of α and β in the models with universally modified Yukawa couplings. If we vary α and β,

TABLE V. The fraction of the VEVs $\tan\beta$ and the scaling factors κ_f and κ_V in the extended Higgs sectors with universal Yukawa couplings.

Model	$\tan\beta$	κ_f	κ_V
Doublet-singlet	$\cdots$	$\cos\alpha$	$\cos\alpha$
Type-I THDM	v_0/v_{ext}	$\cos\alpha/\sin\beta = \sin(\beta-\alpha) + \cot\beta\cos(\beta-\alpha)$	$\sin(\beta-\alpha)$
GM	$v_0/(2\sqrt{2}v_{\text{ext}})$	$\cos\alpha/\sin\beta$	$\sin\beta\cos\alpha - \frac{2\sqrt{6}}{3}\cos\beta\sin\alpha$
Doublet-septet	$v_0/(4v_{\text{ext}})$	$\cos\alpha/\sin\beta$	$\sin\beta\cos\alpha - 4\cos\beta\sin\alpha$

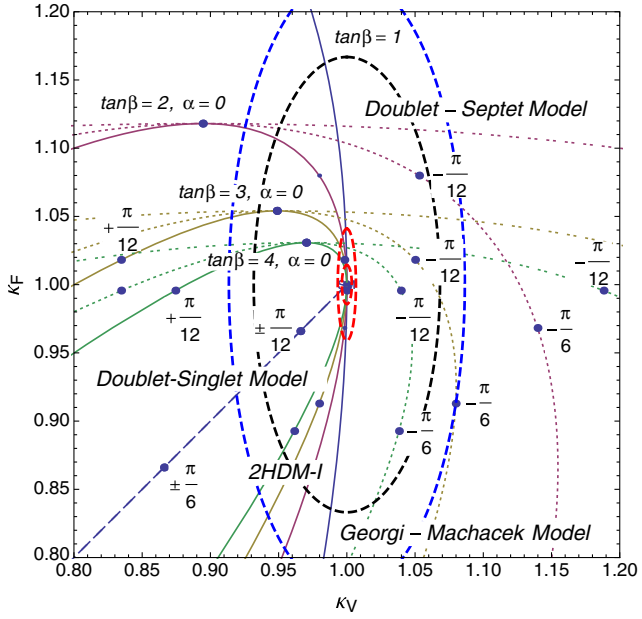

FIG. 12 (color online). The scaling factors κ_f and κ_V in models with universal Yukawa coupling constants.

a model-dependent area (line), which is a distinctive prediction of the models, is drawn. Note that predictions are the same at $\alpha = 0$ in the type-I THDM, the GM model, and the doublet-septet model. From the current LHC data, the scaling factors are obtained at about 20% accuracy at 1σ. It is not sufficient to distinguish these models at this moment. Improvements of the (SM-like) Higgs boson coupling measurements at the HL-LHC and also at the ILC may resolve model predictions.

V. DISCUSSIONS

We here discuss complementarity of precision measurements of the coupling constants of the discovered Higgs boson h and direct searches of additional Higgs bosons at the LHC. In addition, we also discuss the importance of direct searches of additional Higgs bosons at the ILC. A key role is taken by the deviation in the coupling constant of h to weak gauge bosons from the SM prediction, $\delta\kappa_V = 1 - \kappa_V$. When nonzero $\delta\kappa_V$ is found at future colliders, that is identified as an evidence of nonstandard effects mainly due to additional Higgs bosons. By combining the theoretical constraints from perturbative unitarity and vacuum stability, we obtain the upper limit of the energy scale at which evidence of nonstandard Higgs sectors should appear. We first discuss the complementarity in the THDMs and then in the other models later.

For $\delta\kappa_V \gtrsim 5\%$, which is the expected accuracy at the LHC with 300 fb^{-1} [50–52], m_A should be less than about 700 GeV from the conditions of perturbative unitarity and vacuum stability under the assumptions of $m_{H^+} = m_A$ with varying M and m_H in the $m_A \pm 500$ GeV range. In such a case, it is expected that the LHC direct search can find evidence of additional Higgs bosons simultaneously. For $m_A \lesssim 500$ GeV, direct production at the ILC experiment with $\sqrt{s} = 1$ TeV will also be useful to explore the properties of additional Higgs bosons [59]. On top of above, the precision measurement of the couplings of h at the ILC will be the most powerful tool to discriminate types of Yukawa interaction as shown in Figs. 10 and 11.

For $\delta\kappa_V \gtrsim 0.4\%$, which is the expected accuracy at the ILC with $\sqrt{s} = 500$ GeV and $\mathcal{L} = 500$ fb^{-1} [50–52], m_A should be less than 1 TeV from the conditions of perturbative unitarity and vacuum stability under the assumptions of $m_{H^+} = m_A$ with varying M and m_H in the $m_A \pm 500$ GeV range. In such a case, there is a possibility that the direct search at the LHC cannot find any evidence of additional Higgs bosons. In other words, the LHC direct search combined with the constraints from perturbative unitarity and vacuum stability cannot exclude the extended Higgs sector that predicts $\delta\kappa_V \lesssim 0.4\%$. At the ILC, at least the precision measurement of the couplings of h can indicate evidence of the extended Higgs sector. Even in such a situation, as we have shown in the last section, the model discrimination and parameter determination will be still possible by using only the fingerprinting of the deviation of the couplings of h. Furthermore, an upper limit of the mass scale of additional Higgs bosons can be set by the constraints from perturbative unitarity and vacuum stability, while the lower limit is given by the direct search at the LHC. Therefore, we could conclude the existence of the nonstandard Higgs sector at a certain energy scale. This energy scale will be crucial information to design next-generation future colliders.

The accuracy of the $\delta\kappa_V$ measurement can be improved at the ILC with 1 TeV and 1 ab^{-1}, and the indirect upper limit of the mass scale can be slightly extended accordingly. For $\delta\kappa_V \lesssim 0.2\%$, which is beyond the accuracy of the coupling measurement of h at the ILC with $\sqrt{s} =$ 1 TeV and $\mathcal{L} = 1$ ab^{-1} [50–52], the upper limit of the mass scale cannot be obtained from the conditions of perturbative unitarity and vacuum stability. In this case, we cannot separate the extended Higgs sector from the SM from the coupling measurements of h. Therefore, the decoupling limit of the extended Higgs sector cannot be excluded. There are possibilities that the additional Higgs bosons can be discovered at the LHC or the ILC, since the small deviation in κ_V does not necessarily mean the large mass of additional Higgs bosons in the extended Higgs sector. We note that the direct production of additional Higgs bosons at the LHC and the ILC also have the power to discriminate the models of extended Higgs sectors, such as the type of Yukawa sector in the THDMs [59], etc.

To compare the precisely measured values of the Higgs boson couplings, precise calculations in each given model are essentially important. One-loop corrections to the hVV coupling constants have been calculated in Ref. [66], and

those to $hf\bar{f}$ coupling constants have been calculated in Ref. [99] in the THDM. Magnitudes of these corrections due to the additional Higgs boson loops are respectively given to be maximally about 1% and 5% for the hVV and $hf\bar{f}$ couplings under the constraint from perturbative unitarity and vacuum stability. Therefore, the pattern of the deviations in the $hf\bar{f}$ shown in Figs. 10 and 11 does not change even including radiative corrections. However, if the $hf\bar{f}$ couplings are determined with an order of 1% accuracy under the situation in which the deviation in hVV couplings is also found, we may be able to determine not only the type of Yukawa interactions but also some inner parameters such as M^2 in the THDMs. In addition to the hVV and $hf\bar{f}$ couplings, one-loop corrections to the hhh coupling, for which the amount can be significant due to the nondecoupling effect of the additional Higgs bosons, are also important. In Refs. [66,100], it has been shown that the size of the correction can be $\mathcal{O}(100)\%$ under the constraint from perturbative unitarity [68] and vacuum stability [69,70]. By studying the correlation among the deviations in the hhh [66,100], $h\gamma\gamma$ [61,101–103], and $hZ\gamma$ [103,104] couplings from the SM predictions, we can extract properties of additional Higgs bosons running in the loop such as the electric charge, the isospin, and the nondecoupling nature.

Finally, we mention models other than the THDMs. In the doublet-singlet model [60], both the hVV and $hf\bar{f}$ coupling constants are suppressed by the same factor. Therefore, $\kappa_V = \kappa_f < 1$ can be indirect evidence for this model. Detection of an additional CP-even scalar boson, for which the Yukawa and gauge interactions are given only from the mixing with the doublet Higgs field, can be a direct search for the model. The GM model [22] and the doublet-septet model [61–63] have a unique pattern of the deviation in the Higgs boson couplings; namely, κ_V can be larger than unity [63], which is a crucial property to identify these models. In addition, multicharged, e.g., doubly charged, Higgs bosons can significantly contribute to the deviation in the loop-induced $h\gamma\gamma$ and $hZ\gamma$ couplings. When multicharged scalar bosons are discovered, it can be a direct test of these models. Phenomenology of such additional scalar bosons has been discussed in the GM model [105–107] and in the doublet-septet model [108] at the LHC. Measuring the $H^{\pm}W^{\mp}Z$ vertex [77,78] is also an important probe as discussed in Sec. II C.

In this paper, we concentrate on the models with $\rho_{\text{tree}} = 1$. However, we here shortly comment on the Higgs triplet model (HTM) as an important example for models with $\rho_{\text{tree}} \neq 1$, because it is deduced from the type-II seesaw mechanism [109]. In the HTM, although deviations in the hVV and $hf\bar{f}$ couplings cannot be so large due to the constraint from the rho parameter, those in the loop-induced $h\gamma\gamma$ [110–113] and $hZ\gamma$ [111–113] couplings can be significant by the doubly charged Higgs boson $H^{\pm\pm}$ loop. The one-loop corrections to the hhh coupling can also be large as calculated in Refs. [27,114] due to the nondecoupling effect of additional Higgs bosons similarly to the THDM. The correlation among the deviations in the decay rate of $h \to \gamma\gamma$ and the hhh coupling constants[10] from the SM values have been investigated in Ref. [27]. A direct search for $H^{\pm\pm}$ can be an important clue to test the model with the $Y = 1$ triplet field, which can decay into the same-sign dilepton [115–120] and the same-sign diboson [121,122] depending on the magnitude of the triplet VEV.[11]

VI. CONCLUSIONS

We have discussed the determination of the extended Higgs sector by combining the direct and indirect searches for additional Higgs bosons at future collider experiments. Direct searches of the additional Higgs bosons provides the clear evidence for extended Higgs sectors. Focusing on the THDM with the softly broken Z_2 symmetry, we have studied the expected exclusion regions in the m_A-$\tan\beta$ plane at the LHC with the 14 TeV run with 300 fb^{-1} and 3000 fb^{-1} data. For the neutral Higgs boson searches, we have shown that the mass scale up to several hundreds GeV to TeV can be explored at the LHC, depending on the type of Yukawa interaction and parameters such as $\tan\beta$ and $\sin(\beta - \alpha)$. For the indirect searches of additional Higgs bosons via coupling constants of the SM-like Higgs bosons, we have considered various models for the extended Higgs sector, such as the THDMs with four types of Yukawa interactions, the doublet-singlet model, the doublet-septet model, and the GM model, as typical models that predict $\rho_{\text{tree}} = 1$. We have demonstrated that there exists a variety of patterns in the deviations in the SM-like Higgs boson couplings to the gauge bosons and fermions from the SM prediction depending on the structure of the Higgs sector. Therefore, we can fingerprint the nonminimal Higgs sector by detecting the pattern of deviations in an excellent precision at future colliders.

Taking into account the theoretical constraints on the model, such as perturbative unitarity and vacuum stability, the complementarity between the direct searches and the indirect searches can be understood to identify the nonminimal Higgs sector. Observation of the deviation in the coupling constant of the SM-like Higgs boson to the weak gauge bosons plays a key role, which also affects the strategy of the direct search of additional Higgs bosons at colliders. First of all, we have to keep in mind that there exists a decoupling limit in extended

[10]The deviation in the hhh coupling at the tree level is much suppressed by the triplet VEV similar to the hVV and $hf\bar{f}$ as mentioned above.

[11]If there is a mass difference between $H^{\pm\pm}$ and the singly charged scalar components, the cascade decay of $H^{\pm\pm}$ associated with the W boson is possible [123].

Higgs sectors in the limit of $\delta\kappa_V \to 0$, where the SM is a good description as a low-energy effective theory up to much higher scales than the electroweak scale. On the other hand, if a relatively large deviation of $\delta\kappa_V$ is observed, the mass scale of the additional Higgs bosons is bounded from the above by using the argument of perturbative unitarity and vacuum stability so that the direct discovery of them can be highly expected. If a small deviation is observed at the ILC, the direct discovery of the additional Higgs boson can be difficult. Even in such a situation, the fingerprinting of the SM-like Higgs boson couplings can be a solid and powerful tool to explore the extended Higgs sector.

ACKNOWLEDGMENTS

S. K. was supported in part by Grant-in-Aid for Scientific Research from Japan Society for the Promotion of Science (JSPS), Grants No. 22244031 and No. 24340046, and from Ministry of Education, Culture, Sports, Science and Technology (MEXT), Japan, Grant No. 23104006. K. T. was supported in part by MEXT, Grants No. 26104704 and No. 23104011. K. Y. was supported in part by the National Science Council of R. O. C. under Grant No. NSC-101-2811-M-008-014. The work of H. Y. was supported in part by Grant-in-Aid for Scientific Research, Grant No. 24340046, and the Sasakawa Scientific Research Grant from the Japan Science Society.

[1] ATLAS Collaboration, Phys. Lett. B **716**, 1 (2012); CMS Collaboration, Phys. Lett. B **716**, 30 (2012).
[2] ATLAS Collaboration, Report No. ATLAS-CONF-2013-034; CMS Collaboration, Report No. CMS-PAS-HIG-13-005.
[3] G. Aad *et al.* (ATLAS Collaboration), Phys. Lett. B **726**, 88 (2013); **726**, 120 (2013); S. Chatrchyan *et al.* (CMS Collaboration), J. High Energy Phys. 01 (2014) 096.
[4] S. Chatrchyan *et al.* (CMS Collaboration), Phys. Rev. D **89**, 092007 (2014).
[5] S. Weinberg, Phys. Rev. D **13**, 974 (1976); **19**, 1277 (1979).
[6] E. Gildener and S. Weinberg, Phys. Rev. D **13**, 3333 (1976); E. Gildener, Phys. Rev. D **14**, 1667 (1976).
[7] L. Susskind, Phys. Rev. D **20**, 2619 (1979).
[8] H. E. Haber and G. L. Kane, Phys. Rep. **117**, 75 (1985).
[9] J. F. Gunion, H. E. Haber, G. L. Kane, and S. Dawson, Front. Phys. **80**, 1 (2000).
[10] G. Aad *et al.* (ATLAS Collaboration), J. High Energy Phys. 02 (2013) 095.
[11] CMS Collaboration, Report No. CMS-PAS-HIG-13-021.
[12] S. Chatrchyan *et al.* (CMS Collaboration), Phys. Lett. B **722**, 207 (2013).
[13] ATLAS Collaboration, Report No. ATLAS-CONF-2013-027.
[14] CMS Collaboration, Report No. CMS-PAS-HIG-13-025.
[15] G. Aad *et al.* (ATLAS Collaboration), J. High Energy Phys. 06 (2012) 039.
[16] ATLAS Collaboration, Report No. ATLAS-CONF-2013-090.
[17] G. Aad *et al.* (ATLAS Collaboration), Eur. Phys. J. C **73**, 2465 (2013).
[18] G. Aad *et al.* (ATLAS Collaboration), Eur. Phys. J. C **72**, 2244 (2012); S. Chatrchyan *et al.* (CMS Collaboration), Eur. Phys. J. C **72**, 2189 (2012).
[19] G. Aad *et al.* (ATLAS Collaboration), Phys. Rev. Lett. **112**, 201802 (2014); S. Chatrchyan *et al.* (CMS Collaboration), Eur. Phys. J. C **74**, 2980 (2014).
[20] J. Beringer *et al.* (Particle Data Group), Phys. Rev. D **86**, 010001 (2012).
[21] K. Hally, H. E. Logan, and T. Pilkington, Phys. Rev. D **85**, 095017 (2012); K. Earl, K. Hartling, H. E. Logan, and T. Pilkington, Phys. Rev. D **88**, 015002 (2013).
[22] H. Georgi and M. Machacek, Nucl. Phys. **B262**, 463 (1985); M. S. Chanowitz and M. Golden, Phys. Lett. **B165**, 105 (1985).
[23] P. Sikivie, L. Susskind, M. B. Voloshin, and V. I. Zakharov, Nucl. Phys. **B173**, 189 (1980).
[24] T. Blank and W. Hollik, Nucl. Phys. **B514**, 113 (1998).
[25] P. H. Chankowski, S. Pokorski, and J. Wagner, Eur. Phys. J. C **50**, 919 (2007); M.-C. Chen, S. Dawson, and C. B. Jackson, Phys. Rev. D **78**, 093001 (2008).
[26] S. Kanemura and K. Yagyu, Phys. Rev. D **85**, 115009 (2012).
[27] M. Aoki, S. Kanemura, M. Kikuchi, and K. Yagyu, Phys. Rev. D **87**, 015012 (2013).
[28] J. F. Gunion, R. Vega, and J. Wudka, Phys. Rev. D **43**, 2322 (1991).
[29] D. Toussaint, Phys. Rev. D **18**, 1626 (1978); S. Bertolini, Nucl. Phys. **B272**, 77 (1986); W. Hollik, Z. Phys. C **32**, 291 (1986); **37**, 569 (1988).
[30] W. Grimus, L. Lavoura, O. M. Ogreid, and P. Osland, Nucl. Phys. **B801**, 81 (2008); Phys. Lett. B **704**, 303 (2011).
[31] J.-M. Gerard and M. Herquet, Phys. Rev. Lett. **98**, 251802 (2007).
[32] E. Cervero and J. M. Gerard, Phys. Lett. B **712**, 255 (2012).
[33] D. Lopez-Val and J. Sola, Eur. Phys. J. C **73**, 2393 (2013).
[34] M. E. Peskin and J. D. Wells, Phys. Rev. D **64**, 093003 (2001).
[35] S. Kanemura, Y. Okada, H. Taniguchi, and K. Tsumura, Phys. Lett. B **704**, 303 (2011).
[36] S. L. Glashow and S. Weinberg, Phys. Rev. D **15**, 1958 (1977).
[37] V. D. Barger, J. L. Hewett, and R. J. N. Phillips, Phys. Rev. D **41**, 3421 (1990).
[38] Y. Grossman, Nucl. Phys. **B426**, 355 (1994).
[39] A. G. Akeroyd, Phys. Lett. B **377**, 95 (1996).

[40] M. Aoki, S. Kanemura, K. Tsumura, and K. Yagyu, Phys. Rev. D **80**, 015017 (2009).
[41] H. E. Logan and D. MacLennan, Phys. Rev. D **79**, 115022 (2009).
[42] H. E. Logan and D. MacLennan, Phys. Rev. D **81**, 075016 (2010).
[43] G. C. Branco, P. M. Ferreira, L. Lavoura, M. N. Rebelo, M. Sher, and J. P. Silva, Phys. Rep. **516**, 1 (2012).
[44] J. Liu and L. Wolfenstein, Nucl. Phys. **B289**, 1 (1987).
[45] E. Ma, Phys. Rev. Lett. **86**, 2502 (2001).
[46] T. Appelquist and J. Carazzone, Phys. Rev. D **11**, 2856 (1975).
[47] ATLAS Collaboration, arXiv:1307.7292; CMS Collaboration, arXiv:1307.7135.
[48] ATLAS Collaboration, Report No. ATL-PHYS-PUB-2013-014; Report No. ATL-PHYS-PUB-2013-015; Report No. ATL-PHYS-PUB-2014-006.
[49] ATLAS Collaboration, Report No. ATL-PHYS-PUB-2013-016.
[50] H. Baer *et al.* arXiv:1306.6352.
[51] D. M. Asner *et al.*, arXiv:1310.0763.
[52] S. Dawson *et al.*, arXiv:1310.8361v2.
[53] N. Craig, J. Galloway, and S. Thomas, arXiv:1305.2424.
[54] J. Baglio, O. Eberhardt, U. Nierste, and M. Wiebusch, Phys. Rev. D **90**, 015008 (2014).
[55] B. Coleppa, F. Kling, and S. Su, arXiv:1404.1922.
[56] C.-W. Chiang and K. Yagyu, J. High Energy Phys. 07 (2013) 160.
[57] P. M. Ferreira, J. F. Gunion, H. E. Haber, and R. Santos, Phys. Rev. D **89**, 115003 (2014).
[58] H. S. Cheon and S. K. Kang, J. High Energy Phys. 09 (2013) 085; N. Craig and S. Thomas, J. High Energy Phys. 11 (2012) 083; W. Altmannshofer, S. Gori, and G. D. Kribs, Phys. Rev. D **86**, 115009 (2012); S. Chang, S. K. Kang, J.-P. Lee, K. Y. Lee, S. C. Park, and J. Song, J. High Energy Phys. 05 (2013) 075; Y. Bai, V. Barger, L. L. Everett, and G. Shaughnessy, Phys. Rev. D **87**, 115013 (2013); A. Drozd, B. Grzadkowski, J. F. Gunion, and Y. Jiang, J. High Energy Phys. 05 (2013) 072; J. Chang, K. Cheung, P.-Y. Tseng, and T.-C. Yuan, Phys. Rev. D **87**, 035008 (2013); P. M. Ferreira, R. Santos, H. E. Haber, and J. P. Silva, Phys. Rev. D **87**, 055009 (2013); C.-Y. Chen and S. Dawson, Phys. Rev. D **87**, 055016 (2013); A. Celis, V. Ilisie, and A. Pich, J. High Energy Phys. 07 (2013) 053; B. Grinstein and P. Uttayarat, J. High Energy Phys. 06 (2013) 09409 (2013) 110(E); C.-Y. Chen, S. Dawson, and M. Sher, Phys. Rev. D **88**, 015018 (2013); O. Eberhardt, U. Nierste, and M. Wiebusch, J. High Energy Phys. 07 (2013) 118; R. V. Harlander, S. Liebler, and T. Zirke, J. High Energy Phys. 02 (2014) 023; N. Chen, C. Du, Y. Fang, and L.-C. Lü, Phys. Rev. D **89**, 115006 (2014); B. Coleppa, F. Kling, and S. Su, J. High Energy Phys. 01 (2014) 161; L. Wang and X.-F. Han, arXiv:1404.7437; B. Dumont, J. F. Gunion, Y. Jiang, and S. Kraml, Phys. Rev. D **90**, 035021 (2014).
[59] S. Kanemura, H. Yokoya, and Y.-J. Zheng, Nucl. Phys. **B886**, 524 (2014).
[60] V. Barger, P. Langacker, M. McCaskey, M. J. Ramsey-Musolf, and G. Shaughnessy, Phys. Rev. D **77**, 035005 (2008).
[61] J. R. Ellis, M. K. Gaillard, and D. V. Nanopoulos, Nucl. Phys. **B106**, 292 (1976).
[62] J. Hisano and K. Tsumura, Phys. Rev. D **87**, 053004 (2013).
[63] S. Kanemura, M. Kikuchi, and K. Yagyu, Phys. Rev. D **88**, 015020 (2013).
[64] P. P. Giardino, K. Kannike, I. Masina, M. Raidal, and A. Strumia, J. High Energy Phys. 05 (2014) 046.
[65] J. F. Gunion and H. E. Haber, Phys. Rev. D **67**, 075019 (2003).
[66] S. Kanemura, Y. Okada, E. Senaha, and C.-P. Yuan, Phys. Rev. D **70**, 115002 (2004).
[67] H. Huffel and G. Pocsik, Z. Phys. C **8**, 13 (1981); J. Maalampi, J. Sirkka, and I. Vilja, Phys. Lett. B **265**, 371 (1991).
[68] S. Kanemura, T. Kubota, and E. Takasugi, Phys. Lett. B **313**, 155 (1993); A. G. Akeroyd, A. Arhrib, and E. M. Naimi, Phys. Lett. B **490**, 119 (2000); I. F. Ginzburg and I. P. Ivanov, Phys. Rev. D **72**, 115010 (2005).
[69] N. G. Deshpande and E. Ma, Phys. Rev. D **18**, 2574 (1978); M. Sher, Phys. Rep. **179**, 273 (1989); S. Nie and M. Sher, Phys. Lett. B **449**, 89 (1999);
[70] S. Kanemura, T. Kasai, and Y. Okada, Phys. Lett. B **471**, 182 (1999).
[71] N. Chakrabarty, U. K. Dey, and B. Mukhopadhyaya, arXiv:1407.2145.
[72] S. Kanemura, S. Moretti, Y. Mukai, R. Santos, and K. Yagyu, Phys. Rev. D **79**, 055017 (2009).
[73] H. Fusaoka and Y. Koide, Phys. Rev. D **57**, 3986 (1998).
[74] M. Capdequi Peyranere, H. E. Haber, and P. Irulegui, Phys. Rev. D **44**, 191 (1991).
[75] S. Kanemura, Phys. Rev. D **61**, 095001 (2000); Eur. Phys. J. C **17**, 473 (2000).
[76] J. A. Grifols and A. Mendez, Phys. Rev. D **22**, 1725 (1980).
[77] E. Asakawa and S. Kanemura, Phys. Lett. B **626**, 111 (2005); E. Asakawa, S. Kanemura, and J. Kanzaki, Phys. Rev. D **75**, 075022 (2007); S. Godfrey and K. Moats, Phys. Rev. D **81**, 075026 (2010).
[78] S. Kanemura, K. Yagyu, and K. Yanase, Phys. Rev. D **83**, 075018 (2011).
[79] https://twiki.cern.ch/twiki/bin/view/LHCPhysics/CERNYellowReportPageAt14TeV.
[80] A. Pukhov *et al.*, arXiv:hep-ph/9908288.
[81] J. Pumplin, D. R. Stump, J. Huston, H. L. Lai, P. M. Nadolsky, and W. K. Tung, J. High Energy Phys. 07 (2002) 012.
[82] G. Aad *et al.* (ATLAS Collaboration), arXiv:0901.0512.
[83] E. Richter-Was, D. Froidevaux, F. Gianotti, L. Poggioli, D. Cavalli, and S. Resconi, Int. J. Mod. Phys. A **13**, 1371 (1998).
[84] S. Kanemura, K. Tsumura, and H. Yokoya, Phys. Rev. D **85**, 095001 (2012); arXiv:1201.6489.
[85] T. Sjostrand, S. Mrenna, and P. Z. Skands, J. High Energy Phys. 05 (2006) 026.
[86] S. Jadach, Z. Was, R. Decker, and J. H. Kuhn, Comput. Phys. Commun. **76**, 361 (1993).
[87] D. Cavalli and S. Resconi, Report No. ATL-PHYS-98-118.
[88] M. Ciuchini, E. Franco, G. Martinelli, L. Reina, and L. Silvestrini, Phys. Lett. B **334**, 137 (1994); M. Ciuchini,

G. Degrassi, P. Gambino, and G. F. Giudice, Nucl. Phys. **B527**, 21 (1998); F. Borzumati and C. Greub, Phys. Rev. D **58**, 074004 (1998); P. Gambino and M. Misiak, Nucl. Phys. **B611**, 338 (2001).
[89] T. Hermann, M. Misiak, and M. Steinhauser, J. High Energy Phys. 11 (2012) 036.
[90] W.-S. Hou, Phys. Rev. D **48**, 2342 (1993); Y. Grossman and Z. Ligeti, Phys. Lett. B **332**, 373 (1994); Y. Grossman, H. E. Haber, and Y. Nir, Phys. Lett. B **357**, 630 (1995); A. G. Akeroyd and S. Recksiegel, J. Phys. G **29**, 2311 (2003).
[91] M. Krawczyk and D. Sokolowska, *Proceedings of the LCWS2007 and ILC2007 Hamburg, Germany, 2007*, eConf C 0705302, HIG09 (2007).
[92] W. Hollik and T. Sack, Phys. Lett. B **284**, 427 (1992); M. Krawczyk and D. Temes, Eur. Phys. J. C **44**, 435 (2005).
[93] H. E. Haber, G. L. Kane, and T. Sterling, Nucl. Phys. **B161**, 493 (1979).
[94] M. Krawczyk and J. Zochowski, Phys. Rev. D **55**, 6968 (1997).
[95] F. Mahmoudi and O. Stal, Phys. Rev. D **81**, 035016 (2010).
[96] S. Kanemura, K. Tsumura, and H. Yokoya, Phys. Rev. D **88**, 055010 (2013).
[97] J. L. Feng and T. Moroi, Phys. Rev. D **56**, 5962 (1997); V. D. Barger, T. Han, and J. Jiang, Phys. Rev. D **63**, 075002 (2001); J. F. Gunion, T. Han, J. Jiang, and A. Sopczak, Phys. Lett. B **565**, 42 (2003).
[98] J. F. Gunion, R. Vega, and J. Wudka, Phys. Rev. D **42**, 1673 (1990).
[99] S. Kanemura, M. Kikuchi, and K. Yagyu, Phys. Lett. B **731**, 27 (2014).
[100] S. Kanemura, Y. Okada, and E. Senaha, Phys. Lett. B **606**, 361 (2005).
[101] M. A. Shifman, A. I. Vainshtein, M. B. Voloshin, and V. I. Zakharov, Yad. Fiz. **30**, 1368 (1979); [, Sov. J. Nucl. Phys. **30**, 711 (1979)].
[102] I. F. Ginzburg, M. Krawczyk, and P. Osland, Nucl. Instrum. Methods Phys. Res., Sect. A **472**, 149 (2001); N. Bernal, D. Lopez-Val, and J. Sola, Phys. Lett. B **677**, 39 (2009); P. Posch, Phys. Lett. B **696**, 447 (2011); D. Lopez-Val and J. Sola, Phys. Lett. B **702**, 246 (2011); P. M. Ferreira, R. Santos, M. Sher, and J. P. Silva, Phys. Rev. D **85**, 077703 (2012); **85**, 035020 (2012); A. Arhrib, R. Benbrik, and N. Gaur, Phys. Rev. D **85**, 095021 (2012).
[103] A. Arhrib, M. Capdequi Peyranere, W. Hollik, and S. Penaranda, Phys. Lett. B **579**, 361 (2004).
[104] L. Bergstrom and G. Hulth, Nucl. Phys. **B259**, 137 (1985); [**B276**, 744(E) (1986)].
[105] C. -W. Chiang and K. Yagyu, J. High Energy Phys. 01 (2013) 026.
[106] C. Englert, E. Re, and M. Spannowsky, Phys. Rev. D **87**, 095014 (2013).
[107] C.-W. Chiang, A.-L. Kuo, and K. Yagyu, J. High Energy Phys. 10 (2013) 072.
[108] C. Alvarado, L. Lehman, and B. Ostdiek, J. High Energy Phys. 05 (2014) 150.
[109] T. P. Cheng and L. F. Li, Phys. Rev. D **22**, 2860 (1980); J. Schechter and J. W. F. Valle, Phys. Rev. D **22**, 2227 (1980); G. Lazarides, Q. Shafi, and C. Wetterich, Nucl. Phys. **B181**, 287 (1981); R. N. Mohapatra and G. Senjanovic, Phys. Rev. D **23**, 165 (1981); M. Magg and C. Wetterich, Phys. Lett. B **94**, 61 (1980).
[110] P. Fileviez Perez, H. H. Patel, M. J. Ramsey-Musolf, and K. Wang, Phys. Rev. D **79**, 055024 (2009); A. Arhrib, R. Benbrik, M. Chabab, G. Moultaka, and L. Rahili, J. High Energy Phys. 04 (2012) 136; A. G. Akeroyd and S. Moretti, Phys. Rev. D **86**, 035015 (2012); E. J. Chun, H. M. Lee, and P. Sharma, J. High Energy Phys. 11 (2012) 106; L. Wang and X.-F. Han, Phys. Rev. D **87**, 015015 (2013).
[111] C.-W. Chiang and K. Yagyu, Phys. Rev. D **87**, 033003 (2013).
[112] P. S. Bhupal Dev, D. K. Ghosh, N. Okada, and I. Saha, J. High Energy Phys. 03 (2013) 150; 05 (2013) 049(E).
[113] C.-S. Chen, C.-Q. Geng, D. Huang, and L.-H. Tsai, Phys. Lett. B **723**, 156 (2013).
[114] M. Aoki, S. Kanemura, M. Kikuchi, and K. Yagyu, Phys. Lett. B **714**, 279 (2012).
[115] M. Muhlleitner and M. Spira, Phys. Rev. D **68**, 117701 (2003).
[116] A. G. Akeroyd and M. Aoki, Phys. Rev. D **72**, 035011 (2005).
[117] M. Kadastik, M. Raidal, and L. Rebane, Phys. Rev. D **77**, 115023 (2008); J. Garayoa and T. Schwetz, J. High Energy Phys. 03 (2008) 009; A. G. Akeroyd, M. Aoki, and H. Sugiyama, Phys. Rev. D **77**, 075010 (2008).
[118] A. G. Akeroyd and C.-W. Chiang, Phys. Rev. D **80**, 113010 (2009); F. del Aguila and J. A. Aguilar-Saavedra, Nucl. Phys. **B813**, 22 (2009); A. G. Akeroyd, C. W. Chiang, and N. Gaur, J. High Energy Phys. 11 (2010) 005.
[119] E. J. Chun and P. Sharma, J. High Energy Phys. 08 (2012) 162.
[120] H. Sugiyama, K. Tsumura, and H. Yokoya, Phys. Lett. B **717**, 229 (2012).
[121] T. Han, B. Mukhopadhyaya, Z. Si, and K. Wang, Phys. Rev. D **76**, 075013 (2007); P. Fileviez Perez, T. Han, G.-y. Huang, T. Li, and K. Wang, Phys. Rev. D **78**, 015018 (2008); C.-W. Chiang, T. Nomura, and K. Tsumura, Phys. Rev. D **85**, 095023 (2012); Z. Kang, J. Li, T. Li, Y. Liu, and G.-Z. Ning, arXiv:1404.5207.
[122] S. Kanemura, K. Yagyu, and H. Yokoya, Phys. Lett. B **726**, 316 (2013).
[123] M. Aoki, S. Kanemura, and K. Yagyu, Phys. Rev. D **85**, 055007 (2012).